Geomorphology 408 (2022) 108249

Contents lists available at ScienceDirect

Geomorphology

journal homepage: www.journals.elsevier.com/geomorphology

Investigation of the Luco dei Marsi DSGSD revealing the first evidence of a basal shear zone in the central Apennine belt (Italy)

Emiliano Di Luzio [a,*], Marco Emanuele Discenza [b], Diego Di Martire [c], Maria Luisa Putignano [a], Mariacarmela Minnillo [b], Carlo Esposito [d], Gabriele Scarascia Mugnozza [d]

[a] CNR-IGAG, Consiglio Nazionale delle Ricerche, Istituto di Geologia Ambientale e Geoingegneria, Montelibretti, Via Salaria Km 29.3, 00165, Monterotondo St., Rome, (Italy)
[b] Geoservizi S.r.l., Via Luigi e Nicola Marinelli, 86025 Ripalimosani, Italy
[c] Università di Napoli "Federico II", Distar Dipartimento di Scienze della Terra, dell'Ambiente e delle Risorse, Via Cinthia, 21 - 80126 Napoli, Italy
[d] "Sapienza" University of Rome, Department of Earth Sciences and Research Center for Geological Risks (CERI), Piazzale Aldo Moro, 5, 00185. Rome, Italy

ARTICLE INFO

Keywords:
Basal Shear Zone
Slope Tectonics
DInSAR
Central Apennines
Italy

ABSTRACT

Deep-seated gravitational slope deformations (DSGSDs) show a wide range of geomorphological characteristics and kinematic behaviours. In many cases, deforming rock masses move on a continuous surface or a thick basal shear zone (BSZ) overlying the stable bedrock. The nature of this boundary is a significant issue in scientific debates since examples of BSZs have been observed or inferred in some DSGSDs worldwide. In the central Apennines, although several cases of DSGSDs have been described in recent decades, no evidence of BSZs has been documented thus far.

This work presents the first case of a BSZ found in the region at the bottom of a large-scale gravitational deformation that affects the Mesozoic-Cenozoic carbonate ridge overhanging the Luco dei Marsi village (Abruzzi region). The BSZ consists of several metres-thick, cataclastic breccia developed within middle-Upper Cretaceous biodetritic limestone. The breccia level is exposed for approximately 200 m with a subhorizontal geometry and shows severe rock damage and weathering.

The DSGSD hosting the BSZ affects an NNW-SSE-oriented and wide Miocene anticline whose eastern limb is dismembered by Pliocene-Quaternary normal faults delimiting the edge of a large Quaternary intermontane basin (the Fucino Basin). Field survey, aerial photointerpretation, and remote sensing (DInSAR technique) analyses outline an active gravity-driven process. This is characterized by several kinds of geomorphological features, including downhill- and uphill-facing scarps, ridge-top depressions, gravitational grabens and trenches in the upper and middle parts of the ridge, and bulging at the toe of the slope. These features, which can be distinguished from tectonic elements due to their shape and extension, are an indication of a high degree of internal deformation and a compound sagging geometry for the Luco dei Marsi DSGSD.

The short-term activity of the process was revealed by DInSAR time series covering almost thirty years of satellite datasets, including ERS1/2, ENVISAT, COSMO-SkyMed, and SENTINEL 1 constellations. Strain rates on the order of a few mm/yr were inferred, with a marked difference between different sectors of the DSGSD area. The long-term ($y > 10^2$) lifespan of the DSGSD was framed into a multiple-step conceptual model summarizing the Early Pleistocene-Holocene geological evolution of the area. The model results outline the control exercised by extensional tectonics on DSGSD development, as progressive displacements along normal faults in the latest Pleistocene were the cause of lateral unconfinement at the toe of the slope.

This work further contributes to the increasing knowledge on DSGSDs in the central Apennines and the understanding of the relationship between deformation features induced by slope morphogenesis, such as the BSZ, and Quaternary tectonics within the mountain belt.

* Corresponding author at: Consiglio Nazionale delle Ricerche, Istituto di Geologia Ambientale e Geoingegneria, Montelibretti, Via Salaria Km 29.3, 00165, Monterotondo St., Rome, (Italy).

E-mail addresses: emiliano.diluzio@igag.cnr.it (E. Di Luzio), discenza@geoservizisrl.net (M.E. Discenza), diego.dimartire@unina.it (D. Di Martire), marialuisa.putignano@igag.cnr.it (M.L. Putignano), minnillo@geoservizisrl.net (M. Minnillo), carlo.esposito@uniroma1.it (C. Esposito), gabriele.scarasciamugnozza@uniroma.it (G. Scarascia Mugnozza).

https://doi.org/10.1016/j.geomorph.2022.108249
Received 20 September 2021; Received in revised form 6 April 2022; Accepted 6 April 2022
Available online 10 April 2022
0169-555X/© 2022 Elsevier B.V. All rights reserved.

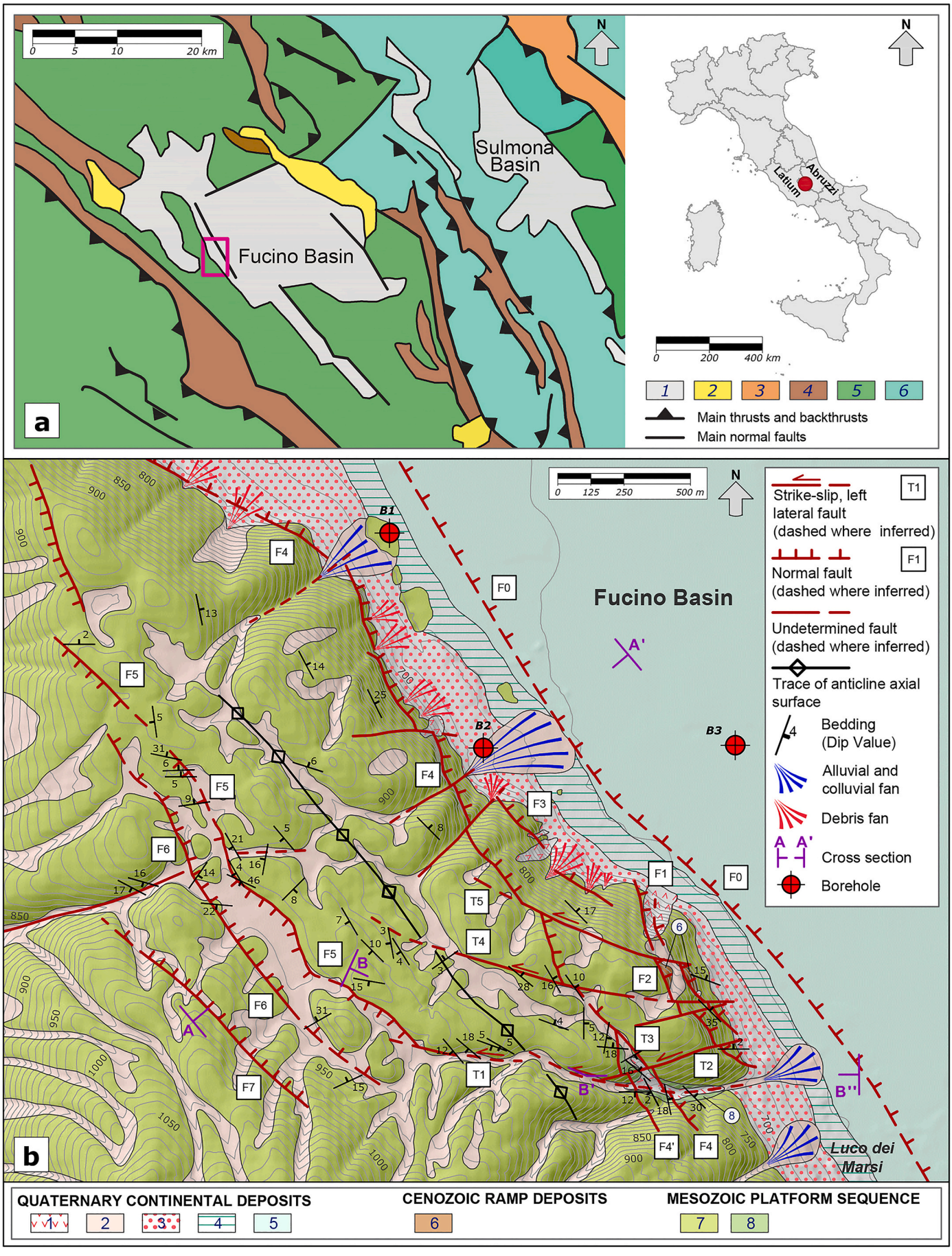

(caption on next page)

Fig. 1. a) Geological map of areas surrounding the Fucino Basin in the axial zone of the central Apennines and location of the study area (purple box). Legend: 1) Quaternary and 2) Lower Pleistocene-Upper Pliocene continental deposits; 3) Lower Pliocene-Upper Miocene and 4) Upper Miocene siliciclastic flysch deposits; 5) Mesozoic-Cenozoic carbonate platform sequence and subordinate Neogene open-ramp deposits; 6) Mesozoic-Cenozoic slope-to-basin carbonate sequences and Neogene open-ramp deposits; and b) geological map of the Luco dei Marsi area. Legend: Quaternary deposits: 1) landslides; 2) residual clay deposits; 3) talus slope deposits; 4) eluvial-colluvial deposits; 5) alluvial and lacustrine deposits of the Fucino Basin; 6) middle Miocene (mM) ramp deposits (*Calcari a Briozoi* and *Lithotamni* Auctt.); and 7) Upper Cretaceous and 8) middle-Upper Cretaceous biodetritic limestone. Borehole B1–B3 data were taken from https://www.isprambiente.gov.it. (For interpretation of the references to color in this figure legend, the reader is referred to the web version of this article.)

1. Introduction

Deep-seated gravitational slope deformations (DSGSDs) are defined as large-scale, slow-moving processes inducing rock mass deformation in large portions of slopes over long time periods (e.g., Zischinsky, 1966; Nemčok, 1972; Mahr, 1977; Hutchinson, 1988; Dramis and Sorriso-Valvo, 1994; Agliardi et al., 2012; Crosta et al., 2013; Discenza and Esposito, 2021). DSGSDs may affect large rock volumes and are revealed, at the mountain scale, by geomorphological evidence distributed over slope-to-valley systems. A great variety of morphostructures and kinematic evolutionary modes are possible, depending on the geological and geomorphological environment as well as morphoclimatic conditions (Radbruch-Hall, 1978; Bovis, 1982; Chigira, 1992; Ambrosi and Crosta, 2011; Bianchi Fasani et al., 2014; Jaboyedoff et al., 2013).

DSGSDs have been recognized in different mountain belts worldwide (see Pánek and Klimeš, 2016; Discenza and Esposito, 2021 for a review), and recent evidence of DSGSDs was detected on Mars (Mège and Bourgeois, 2011; Guallini et al., 2012; Discenza et al., 2021).

Several cases of DSGSDs have also been described in the central sector of the Apennine belt (Crescenti et al., 1987; Dramis et al., 1987; Di Luzio et al., 2004a; Martino et al., 2004; Galadini, 2006; Scarascia Mugnozza et al., 2006; Esposito et al., 2007, 2013, 2014, 2021; Moro et al., 2007, 2009, 2012; Bianchi Fasani et al., 2011, 2014; Discenza et al., 2011; Gori et al., 2014; Della Seta et al., 2017; Del Rio et al., 2021). This is a mountain region with moderate relief landscape and topography, rarely exceeding 2500 m a.s.l. However, a relative elevation of up to 1 km between mountain ridges and valley floors is quite common in the area.

The development of Apennine DSGSDs was mainly conditioned by the post-Early Pleistocene regional uplift of the belt and localized Pliocene-Quaternary normal faulting, both factors controlling the morphogenesis of slope-to-valley systems (Cavinato and De Celles, 1999; D'Agostino et al., 2001; Bartolini et al., 2003; Galadini et al., 2003; Faccenna et al., 2014). Inherited structural elements, which originated during thrust tectonics in the Neogene-Early Pleistocene, also played an important role. Folds, thrusts and *syn*-thrusting normal faults acted as predisposing factors, influencing the size and geometry of DSGSDs (Di Luzio et al., 2004a; Esposito et al., 2007, 2013, 2021; Bianchi Fasani et al., 2014; Della Seta et al., 2017). Moreover, the geometric characteristics of mesoscale discontinuities have been demonstrated to directly influence the rheological properties of jointed rock masses (Discenza et al., 2020). Finally, karst processes can also influence DSGSD activation in the carbonate ridges of the Apennine belt (Martino et al., 2004; Maffei et al., 2005; Discenza et al., 2011; Lenti et al., 2012).

The detection of DSGDs in a tectonically active belt such as the central Apennines also has geohazard- and risk-related implications for two main reasons: the possible triggering of large landslides and catastrophic rock slope failures (Cinti et al., 2001; Di Luzio et al., 2004b; Bianchi Fasani et al., 2014) and the seismic amplification in damaged rock masses that can have a significant impedance contrast with the underlying undeformed bedrock (e.g., Martino et al., 2020).

The main aim of this work is the geomorphological and kinematic (through the DinSAr technique) characterization of a new case study, the Luco dei Marsi DSGSD, thus contributing to the analysis of slope-scale gravitational deformation in the Apennine Mountains and filling the gap in knowledge regarding other mountain belts worldwide. Moreover, the first field evidence of a basal shear zone (BSZ) observed in the mountain belt is presented; a boundary between the deforming rock mass and stable bedrock in large-scale slope deformations. Previous studies have indicated the lack of a continuous sliding surface or basal shear zone as a distinctive feature among landslides and DSGSDs (Dramis and Sorriso-Valvo, 1994; Sorriso-Valvo, 1995). As demonstrated in several studies worldwide (Ambrosi and Crosta, 2006; Bonzanigo et al., 2007; Madritsch and Millen, 2007; Agliardi et al., 2001, 2012, 2019; Barla et al., 2010; Zangerl et al., 2010; Strauhal et al., 2017), many DSGSDs move on a thick and continuous BSZ, which is generally composed of cataclastic breccias with maximum thicknesses of a few tens of metres. However, examples of well-exposed outcrops are very rare, and the description of the BSZ found at the base of the Luco dei Marsi DSGSD can be of general interest worldwide.

The Luco dei Marsi DSGSD affects a carbonate rock slope elongated in a NNW-SSE direction along the western edge of the Fucino Basin, the widest Pliocene-Quaternary tectonic depression in the central Apennines (Fig. 1a).

Therefore, a further objective was to frame the gravity-driven process in the morphotectonic evolution of the local slope-to-basin system over a temporal interval extending from the beginning of the Pleistocene to the historical era. A multiple-step conceptual model of slope evolution was derived from the main geomorphological evidence, including relicts of Pleistocene palaeosurfaces and a review of literature data. The DSGSD should have been activated in the latest Pleistocene when an increase in normal faulting activity along the edge of the slope caused the necessary lateral unconfinement.

2. Geological and geomorphological framework

The Luco dei Marsi ridge extends in the axial zone of the central Apennine belt, which is characterized by NW-SE-oriented carbonate structures overthrusting Neogene flysch deposits (Fig. 1a) because of late Miocene tectonics (Patacca et al., 2008; Cosentino et al., 2010). The mountain ridge is confined to the east by the Fucino Basin (Figs. 1b, 2), a sedimentary depression originating in a continental environment as a consequence of Pliocene-Quaternary normal faulting (Giraudi, 1988; Galadini and Messina, 1994; Bosi et al., 1995, 1996; Cavinato et al., 2002; Galadini et al., 2003).

The structural setting corresponds to a wide, symmetric antiform cut by normal and strike-slip faults (Fig. 3a, b). The backbone of the slope is composed of Upper Cretaceous, shallow-water, biodetritic and well-layered limestone deposited in a carbonate platform environment (Fig. 4a). Laminated, massive beds (2–3 m thick) characterize middle-Upper Cretaceous, biodetritic (rudist-bearing) facies (Fig. 4b) in the southern sector (Fig. 1b), whereas buried Lower Cretaceous limestone crops out a few km south of the study area (Praturlon, 1968). The carbonate sequence ends upwards with middle Miocene open-ramp biodetritic limestone ("*Calcari a Briozoi e Lithotamni*" Auctt.) that unconformably overlies the Upper Cretaceous layers on subvertical cliffs along the edge of the slope (Fig. 4c).

Finally, Quaternary deposits include residual clays originating from karst processes and eluvial-colluvial material filling the main depressions within the Luco dei Marsi ridge (Fig. 4d). Landslide deposits, talus debris and alluvial fans characterize the footslope, whereas the piedmont junction area is covered by colluvial deposits and the lacustrine-alluvial sequence of the Fucino Basin (Fig. 1b).

The fold structure is dissected by NNW-SSE-oriented and mainly ENE-dipping, longitudinal normal faults and fault zones which implied

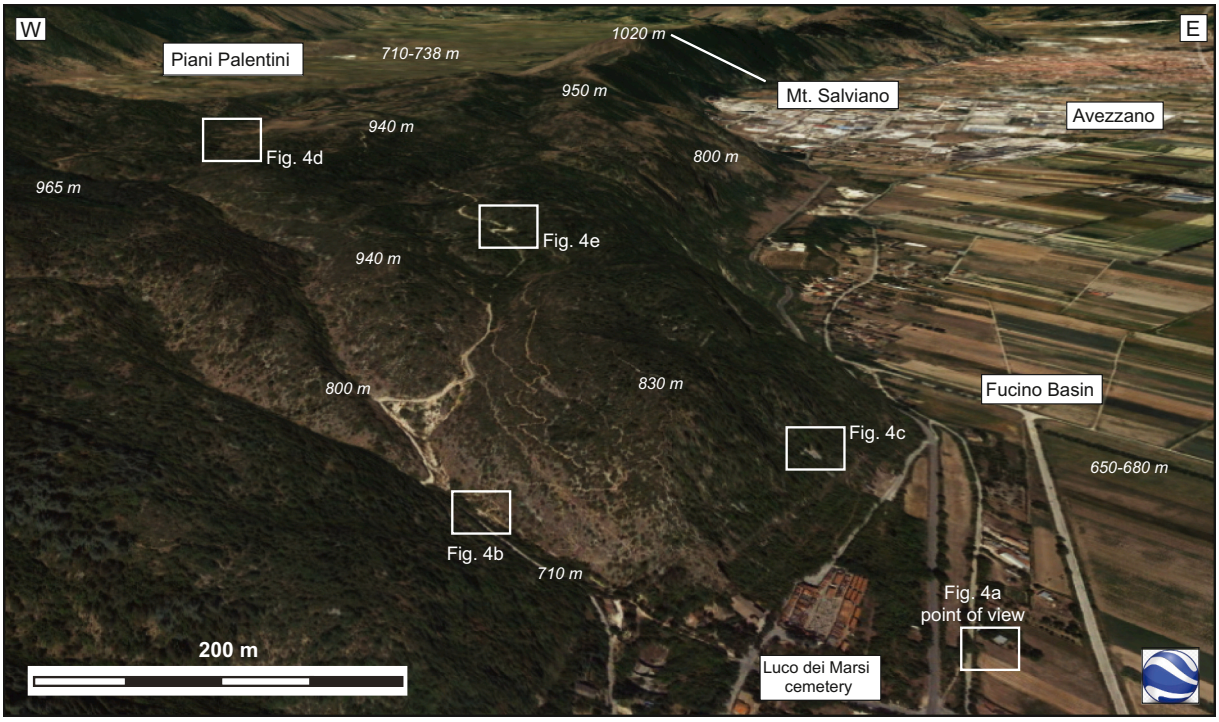

Fig. 2. Google-Earth® view of the Luco dei Marsi-Mt. Salviano ridge along the western edge of the Fucino Basin. Image Landsat/Copernicus, 10/10/2019.

an extension in the ENE-WSW direction without however modifying the main axis of ridge elongation inherited from the Neogene thrusting. In the western areas (F5-F6), such faults generated an elongated (inner) graben (Figs. 1b, 4d), whereas along the eastern boundary of the ridge (F1–F4), they run parallel to the main slope escarpment (Fig. 4a, c). The same fault system includes the Luco dei Marsi Fault (LMF=F0) located within the topographic depression of the Fucino Basin (Figs. 1b, 3a). The tectonic framework is completed by a set of WNW-ESE-oriented, left-lateral strike-slip faults (Fig. 4e) that characterize the southern areas (T1–T5 in Fig. 1b), where they displace the fold axis.

The geomorphological setting of the area is characterized by the Luco dei Marsi-Mt. Salviano ridge that corresponds to the watershed divide between the Fucino Basin (elevation 650–680 m a.s.l.) and the Piano Palentini tableland (710–738 m a.s.l.). The gently eastward-dipping (20–25°) and narrow (1 km-wide) slope of Mt. Salviano (1020 m a.s.l.) progressively widens southward, and westward of Luco dei Marsi is 2 km wide in a W-E direction (Fig. 2). Here, the ridge top is furrowed by elongated and longitudinal valleys, the main morphological depression corresponding to the inner graben (Fig. 5). The eluvial-colluvial infilling is fed by V- and U-shaped transverse and shorter valleys. Secondary ridges, acting as watershed divides of longitudinal valleys, locally present mounded or flattened top surfaces, which were identified as remnants of former paleosurfaces (Fig. 6a–b). These flat areas show moderate extensions and are interrupted by scarps, trenches, or secondary streams (Fig. 5). Moreover, in the upper part of the relief, karst processes are testified by dolines (Fig. 6b) and lacustrine depressions (Fig. 6c). Along the eastern edge of the slope, V-shaped and short transverse valleys are locally truncated by morphological breaks (suspended valleys), which reveal a rejuvenation of the hydrographic network (Fig. 5). Solid transport produced large alluvial and colluvial fans at the slope base, resting with dip angles of 5–10° and up to 400 m long. Smaller debris fans (a few tens of metres long) are linked to gravity-driven and erosional processes and show greater dip angles, between 10 and 15° (Fig. 6d).

Finally, landslides, including rock falls and planar sliding processes, were documented along the lower part of the slope (Fig. 5).

3. Methodologies

Geological and geomorphological maps were obtained through a detailed (1:5000 scale) field survey and interpretation of aerial photo and satellite images (Google Earth®). The aerial photos were taken from flights of different periods: i) “volo Italia” IGMI (Italian Geographic Military Institute) 1954 (1:33,000 scale); ii) “volo Abruzzo region” 1987 (1:33,000 scale), 2002 and 2007 (both 1:5000 scale); and orthophoto Abruzzi region 2010 (1:5000 scale). Most of the evidence of paleosurfaces from the analysis of remote sensing images was later checked in the field.

The processing and interpretation of DInSAR (Differential Interferometric Synthetic Aperture Radar) datasets from the ERS1/2, ENVISAT, COSMO-SkyMed and SENTINEL 1 satellite constellations allow the estimation of the deformation rates of the Luco dei Marsi DSGSD over the last three decades. The DInSAR technique (Franceschetti et al., 1992) has been widely used in detecting displacements of the Earth's surface with subcentimetric accuracy (e.g., Moreira et al., 1995; Bozzano et al., 2017, 2018; Antonielli et al., 2019; Solari et al., 2020). DInSAR is based on the calculation of the phase difference (interferogram) between two images acquired over the same area but at different times along the sensor-target direction (line of sight - LoS). This operation can be made by means of two sensors applied on the same platform or in different periods with the aid of images captured on different satellite orbits. Satellites cover ascending and descending semipolar orbits. Due to Earth rotation and to the fact that SAR antennas are pointed on the same side with respect to the velocity vector in the orbit trajectory, an area can be observed from the east during descending orbits (from north to south) or from the west during ascending orbits.

By utilizing this method, it is possible to obtain mean displacement rate maps and time series of deformations that allow reconstruction of the kinematic evolution of different phenomena, such as landslides, natural and anthropogenic subsidence, volcanic-related ground movements, and coseismic and postseismic deformation, all characterized by low to extremely low displacement rates. DInSAR has also proven to be an effective tool for the investigation of DSGSDs (e.g., Ambrosi and Crosta, 2006; Moro et al., 2009; Barla et al., 2010; Agliardi et al., 2012;

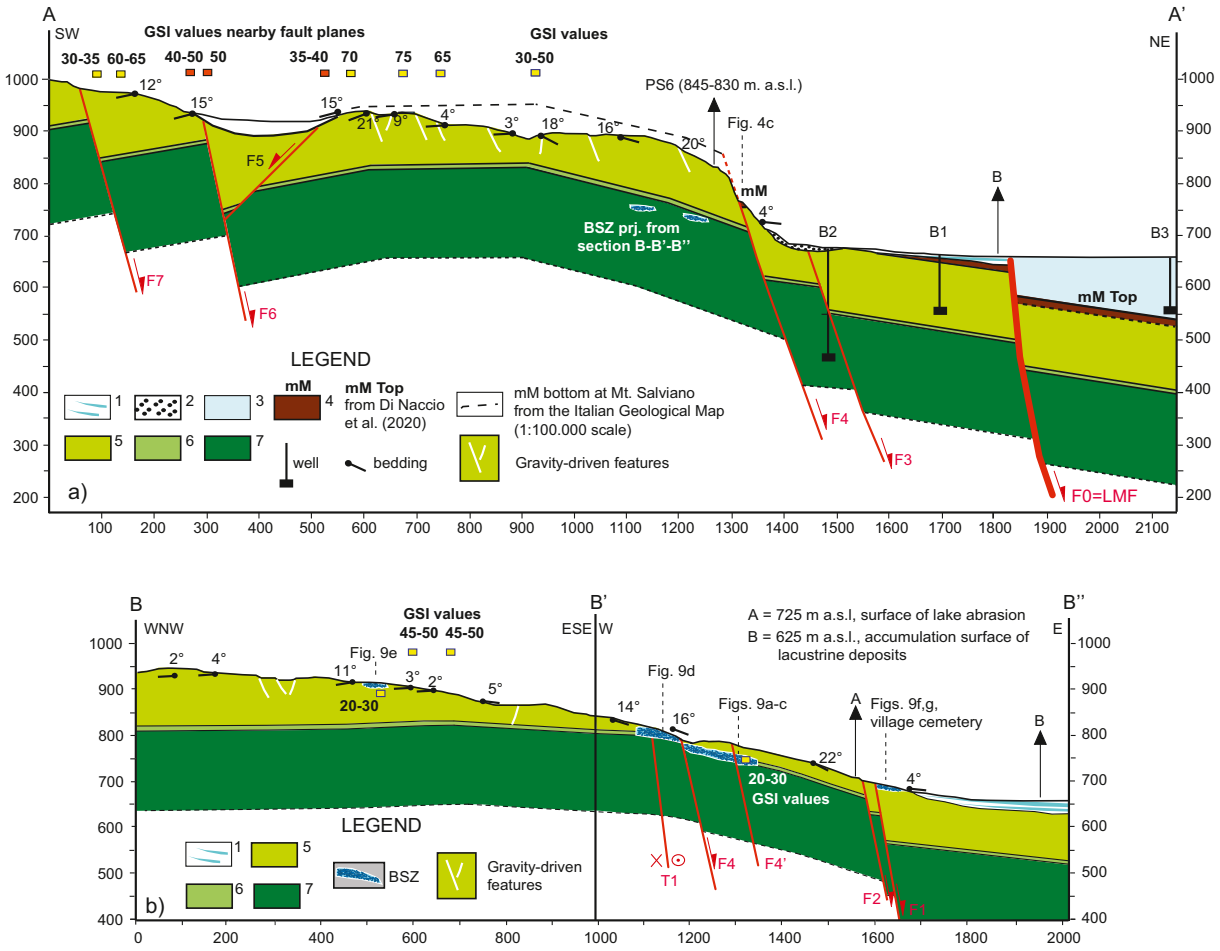

Fig. 3. Geological Cross-sections A-A′ and B-B′-B″ (see traces in Fig. 1b). Legend: 1) alluvial and colluvial fan deposits intercalated with lacustrine deposits (Quaternary); 2) talus deposits (Quaternary); 3) undifferentiated lacustrine and alluvial deposits (Upper Pliocene?-Quaternary); 4) middle Miocene (mM) open ramp deposits; 5) Upper Cretaceous, layered limestone; 6) middle-Upper Cretaceous massive limestone; and 7) Lower Cretaceous limestone. BSZ = basal shear zone. GSI values are reported on both profiles.

Frattini et al., 2013, 2018; Notti et al., 2013; Di Martire et al., 2016; Cappadonia et al., 2019; Delchiaro et al., 2021).

In this research, the analysis of interferometric data over the 1993–2019 period was conducted to assess the present activity and deformation rates of the Luco dei Marsi DSGSD. The study was carried out using datasets from different sources: a) C- and X-band interferometric data acquired from the ERS1/2, ENVISAT and COSMO-SkyMed constellations (for the 1993–2010 and 2011–2014 periods, respectively), both available within the "Not ordinary Plan of Environmental Remote Sensing" (Sacco et al., 2015; Costantini et al., 2017; Di Martire et al., 2017; Geoportale Nazionale, 2017); and b) C-band data obtained from the SENTINEL 1 images for the 2016–2019 period, obtained within the Copernicus program of the European Space Agency.

4. Results

This section illustrates the main geomorphological features ascribed to the Luco dei Marsi DSGSD and which were observed in different parts of the slope, from the ridge top to the eastern edge and the piedmont junction area, also with the help of aerial photo interpretation. In addition, the geometric and textural characteristics of the BSZ are described, together with a basic geomechanical characterization through estimates of the GSI (Geological Strength Index, Hoek and Brown, 1997) values. Finally, the results of the DInSAR data elaboration and analysis are presented, distinguished for three time spans: 1993–2010 (ERS1/2 and ENVISAT constellation), 2011–2014 (COSMO-SkyMed) and 2016–2019 (SENTINEL 1).

4.1. Geomorphological features of the Luco dei Marsi DSGSD

The northern edge of the gravitational deformation was initially identified with an incised SW-NE-oriented and V-shaped rock gully (Fig. 5). However, evidence of ridge splitting and a few trenches north of the gully would indicate a wider extension, without a clear boundary with undeformed rocks (Fig. 7). The southern edge is better detected along a further gully that drains towards Luco dei Marsi with an articulated trend, from WNW-ESE to E-W (Figs. 5, 7). Considering these limitations, the Luco dei Marsi DSGSD spreads over a subrectangular area of approximately 2.4 km^2, with a width of 2.4 km in a NW-SE direction and a length of approximately 0.9 km in the direction of the maximum slope (SW-NE). The elevation difference between the top and slope base is approximately 300 m.

In the highest sector, the gravitational deformation is delimited westwards by a 2-km long, east-dipping, main longitudinal scarp (Fig. 7). Such a 10–20-metre-high rear scarp is partially vegetated, severely degraded, and locally interrupted by transverse morphological elements. Isolated segments of the rear scarps are a few hundred metres in length. Near the La Cucinella church, one of these segments is paired with an uphill-facing scarp, thus originating a ridge-top depression (Fig. 8a). South-east of the La Cucinella church, some secondary scarps follow the main escarpment with a similar orientation and kinematics; these scarps have a reduced planimetric extension and, overall, form a

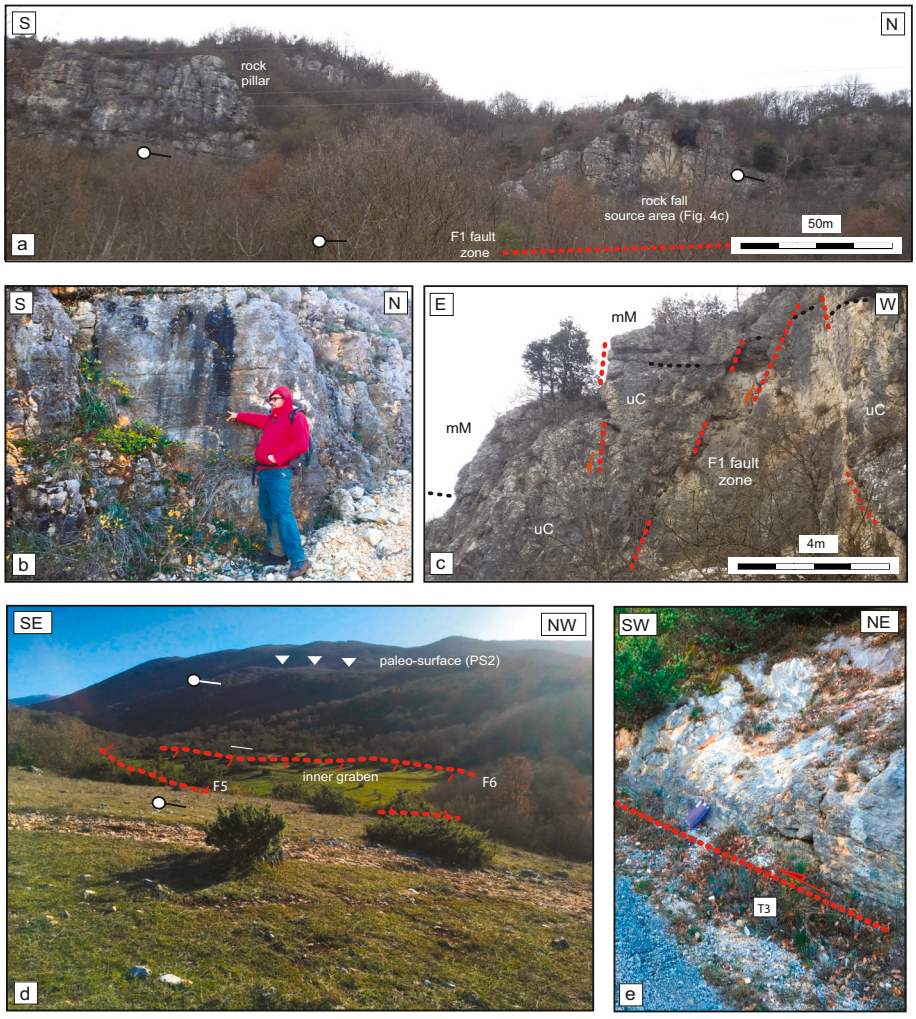

Fig. 4. Geological features: a) longitudinal rock scarps composed of Upper Cretaceous, layered, and jointed limestone on the eastern edge of the Luco dei Marsi slope; b) middle-Upper Cretaceous massive, rudist-bearing, laminated limestone; c) fault zone F1 cutting middle Miocene (mM) and Upper Cretaceous (uC) biodetritic limestone; d) the inner graben filled by Quaternary colluvial and residual deposits; and e) WNW-ESE-oriented, left-lateral, strike-slip fault.

stepped system that displaces the deforming rock mass towards the ENE (Fig. 7).

In the middle portion of the DSGSD, a main longitudinal depression is articulated in four segments (G1–G4 in Fig. 7), 250 to 600 m long and separated by transversal saddles, secondary scarps, and trenches. These areas are bordered on their western sides by a dipslope scarp system and by iso-oriented, uphill-facing scarps on the eastern edges, both varying in height from a few metres to over 10 m (Fig. 8a, b). The four longitudinal structures (G1–G4 in Fig. 7) are identified as grabens of gravitational origin filled with residual deposits and having flat bottom surfaces.

Corresponding to the slope break, secondary scarps and trenches, tens of metres long, isolate rock slabs with volumes of thousands of cubic metres. Within rock slabs, persistent joint systems separate rock pillars prone to fall due to toppling or wedge-sliding failure mechanisms (Fig. 8c). Moreover, within the slabs, the rock mass is fragmented by centimetric-sized extensional fractures, downwards or upwards terminating against subhorizontal shear planes (Fig. 8d); similar deformation patterns were described by Chigira (1992) for hard rock types involved in mass rock creep. Finally, the lowermost part of the slope is affected by bulging, which gives rise to convex morphologies towards the piedmont junction zone and the Fucino Basin (Fig. 8e).

4.2. *Field evidence of the basal shear zone*

The bottom of the DSGSD is marked by a BSZ that was exposed by linear erosion deeply incising the carbonate ridge in the southernmost sector of the study area, west of Luco dei Marsi (Figs. 7, 9a). In the main outcrop, the BSZ was observed at elevations ranging between 750 and 790 m a.s.l. (Fig. 3b). The rock mass resembles a damaged zone composed of cataclastic breccia with a fine matrix (Fig. 9b), which mainly developed within the middle-Upper Cretaceous, massive biodetritic limestone (Fig. 4b).

The cataclastic band has a subhorizontal to gently east-dipping attitude and can be followed in the field for approximately 150 m. The deforming rock mass (DRM) above is clearly affected by wide open and subvertical joints (Fig. 9c). The maximum thickness observed for the BSZ is 5 m, but this could be an underestimated value since the lower part is involved in a landslide process. At a few sites along the rock gully, the BSZ is dislocated by NNW-SSE-oriented normal faults belonging to the longitudinal system featuring the Luco dei Marsi ridge (Fig. 9a, c). Although the vertical downthrow is very low, such evidence is a clue to unravelling the relationship between tectonic processes and gravity-driven deformations, as will be further discussed.

The GSI values estimated for the BSZ are very low, approximately 20–30, typical of heavily broken and poorly interlocked rock masses; rock damage was likely the result of high strain concentration during

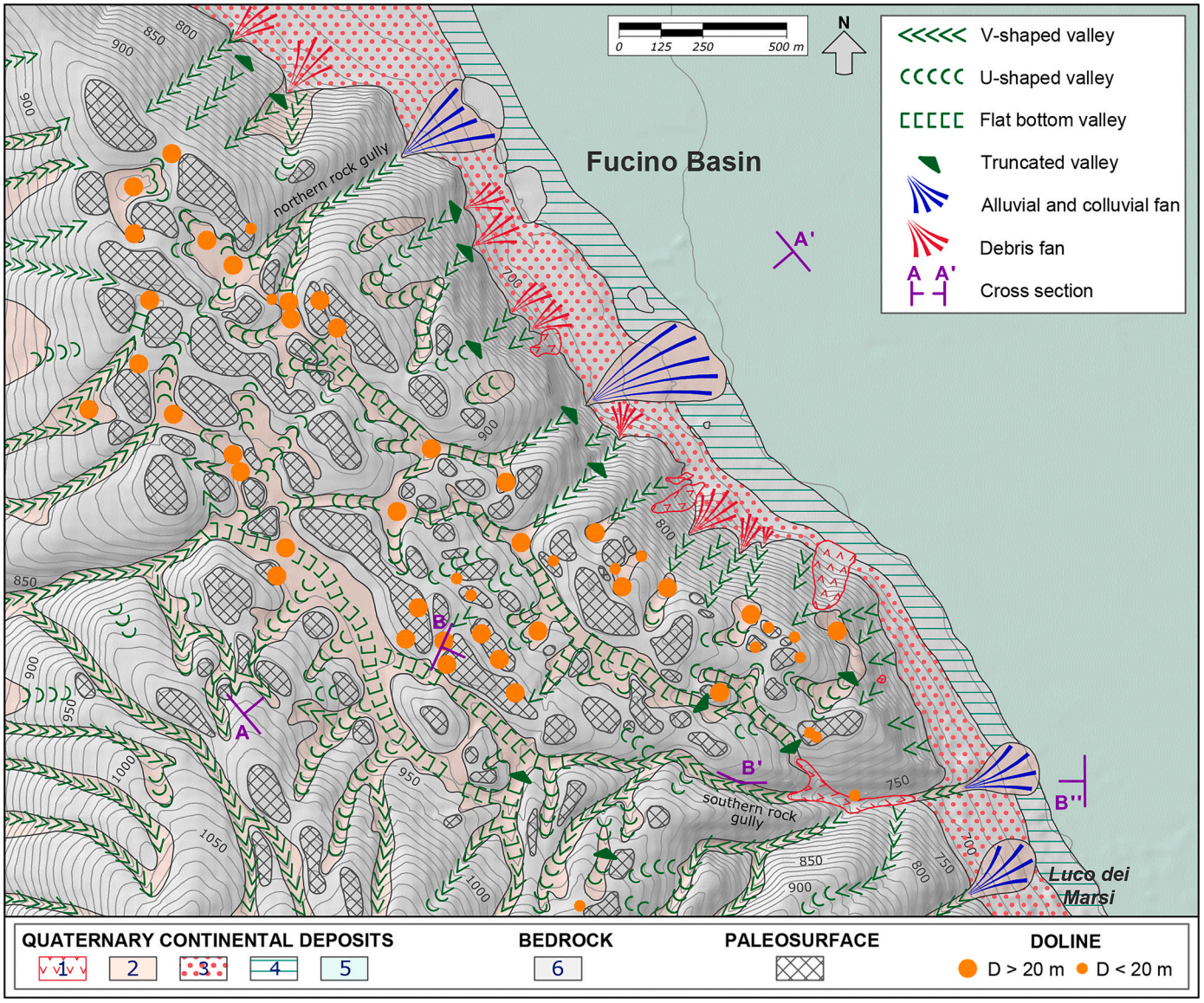

Fig. 5. Geomorphological map of the study area. Legend: Quaternary deposits: 1) landslides; 2) residual clay deposits; 3) talus slope deposits; 4) eluvial-colluvial deposits; and 5) alluvial and lacustrine deposits of the Fucino Basin.

DSGSD onset and development. GSI measurements within other sectors of the DSGSD area range between 60 and 75 (Fig. 3a, b). Approaching the faults bordering the inner graben, GSI values decrease to 35–50 because of the more intense, brittle deformation but never reach the very low values within the BSZ. The weakening of the rock mass within the BSZ is also due to weathering and/or karst processes that originated veins of residual, red clays (Fig. 9d).

Apart from the large outcrop shown in Fig. 9a, c, the BSZ was observed in several small outcrops within the southern rock gully, up to the inner graben. In the uppermost slope sector, at an elevation of 910 m, where the fluvial incision has eroded the bedrock less, the upper zone of the BSZ appears again as a cataclastic breccia with subcentimetric clasts (Fig. 9e). On the opposite side of the DSGSD, the BSZ was found at the base of the Luco dei Marsi ridge, near the village cemetery, at 695 m a.s.l. (Fig. 3b), where the cataclastic zone was recognized in Upper Cretaceous, subhorizontal beds (Fig. 9f, g).

4.3. DInSAR data analysis for the 1993–2010 time span

The data available from the ERS1/2 and ENVISAT constellations allowed the implementation of mean displacement rate maps in the two geometries of acquisition, ascending and descending, for the 1993–2010 time span (Fig. 10a–d). The density and distribution of targets were significantly different between the two geometries. It has been acknowledged (Plank et al., 2012; Cigna et al., 2014) that ground visibility is influenced by the acquisition geometry (incidence and orbit angles) and the morphology of the investigated surface (slope and aspect). In the area of interest, the mountain ridge is exposed to the east, and its average dip is 21°. This combination, together with the incident angle (which for the ERS1/2 and ENVISAT satellites is 23°), induced the phenomenon of foreshortening, which implies an almost orthogonality between the LoS and the slope for descending acquisitions. This is the reason for the scarce presence of reflectors. Slightly better conditions were generated for acquisitions in ascending geometry, whose LoS was subparallel with the aspect of the slopes. In both cases, the thick vegetation cover reduced the number of available reflectors, and displacement rate maps show scattered targets with very low values of deformation rates, rarely exceeding ±1.5 mm/y (Fig. 10a–d).

Displacement rates recorded by both European satellite constellations (ERS1/2 and ENVISAT) are shown in the time series in Fig. 11a–b

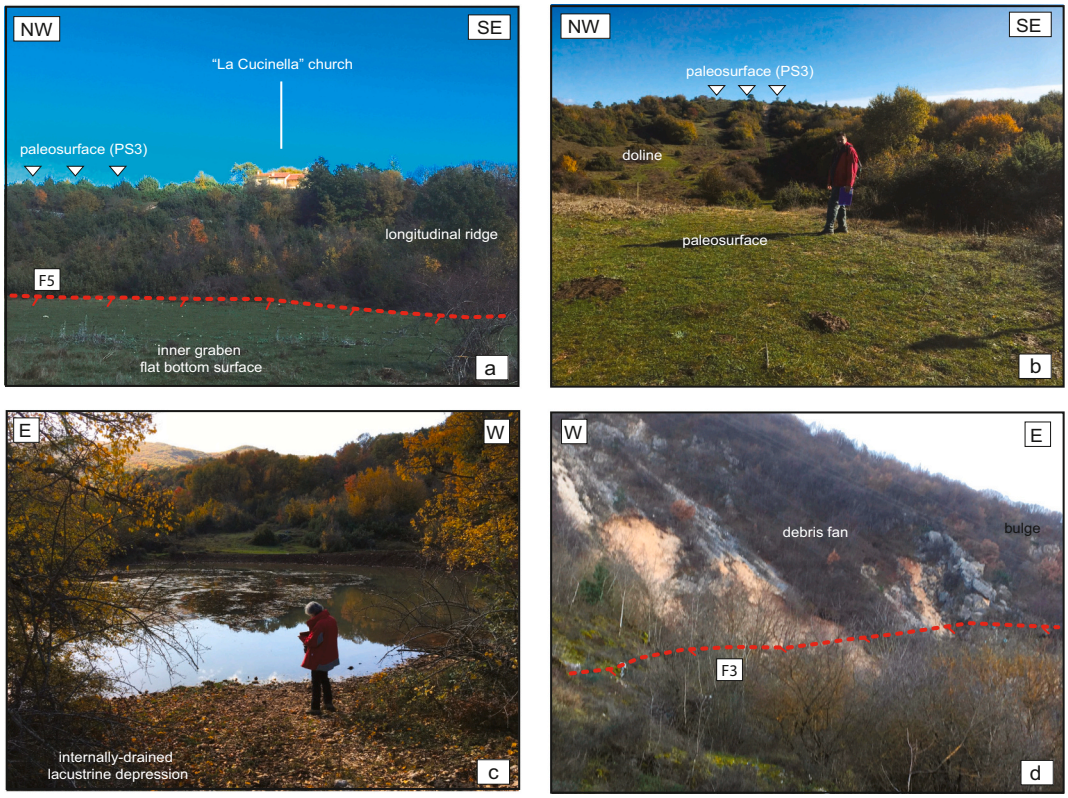

Fig. 6. Geomorphological features: a) top-flattened (longitudinal) ridge along the eastern edge of the inner graben; b) paleosurface and doline (radius approximately 80 m) observed on the ridge top; c) 50 m-wide lacustrine, karst depression; and e) debris fan along the slope base.

for selected targets (T). These were acquired in ascending mode, detected in both constellations, and located in two different sectors of the DSGSD area (Fig. 10a, c) to assess possible differences in terms of displacement. Indeed, while in the central sector targets T1-ers and T1-env showed a substantial stability over the 1993–2010 period (Fig. 11a), in the southern sector slightly higher rates for targets T2-ers and T2-env seemed to be present, and the time-series were characterized by a linear trend on the order of approximately 1.2 mm/y (Fig. 11b).

4.4. DInSAR data analysis for the 2011–2014, 2016–2019 and 1993–2019 time spans

Data acquired by the COSMO-SkyMed constellation of the Italian Space Agency (ASI) over the 2011–2014 period are reported in the descending geometry only (Fig. 12a). It is worth pointing out that, unlike the ERS and ENVISAT satellites, the incident angle for the COSMO-SkyMed satellites is 32°, which allowed a larger number of reflectors to be identified in the investigated area. In this time interval, the displacement map shows low rates (between 1.5 and 3.0 mm/yr) in the central-northern sector, while in the southern sector, slightly higher values (between 3.0 and 5.0 mm/yr) are present, thus confirming the evidence from the processing of the ERS and ENVISAT datasets.

The observation window for displacement rates was extended up to 2019 through an additional 165 SAR images from SENTINEL 1. To ensure continuity with respect to COSMO-SkyMed data (available in descending geometry), only descending images were processed. Such processing was carried out by SUBSIDENCE software, which implemented the Coherent Pixel Technique - Temporal Phase Coherence (CPT-TPC). CPT-TPC was used to obtain ground displacement values from satellite radar images. A detailed description of the whole algorithm can be found in Mora et al. (2003) and Iglesias et al. (2015). As a result, Fig. 12b shows the map of the mean displacement rates for the analysed 2016–2019 period, which again highlights two sectors with different values.

Considering the rather close positions of the selected targets for the various satellite constellations, two cumulative time series were derived combining COSMO-SkyMed, SENTINEL 1, ERS1/2 and ENVISAT data (Fig. 11c, d), thus covering the 1993–2019 period. Almost three decades of observations confirmed the difference between the central-northern and southern sectors of the area affected by the DSGSD: while the former showed a displacement rate less than 1.0 mm/y over the entire time interval, the latter showed a slight linear trend of approximately 1.5 mm/y.

Further time series were derived for two points of particular interest within the DSGSD, near La Cucinella church, a few metres northeast of the main rear scarp (target Tcc in Figs. 8a, 12a, b), and in the BSZ sector (target Tbsz in Fig. 12a, b). Unfortunately, only the COSMO-SkyMed and SENTINEL 1 datasets were available for these points covering the 2011–2019 interval. In both cases, the time series revealed a significant displacement rate, reaching values of approximately 6.5 mm/yr (Fig. 11e) and 6.0 mm/yr (Fig. 11f) for the Tcc and Tbsz targets, respectively.

5. Discussion

This chapter discusses the results of the interferometric (Section 5.1) and geomorphological (Section 5.2) analyses that highlight the short- and long-term kinematics of the DSGSD. Subsequently, an integration of the new data with evidence from the literature is proposed to reconstruct the possible evolution of the local slope-to-basin system in the Quaternary (Section 5.3). Finally, plausible hypotheses on the deformation style of the DSGSD and the significance of the BSZ in the context of the morphotectonic evolution of the Apennine structures are discussed (Section 5.4).

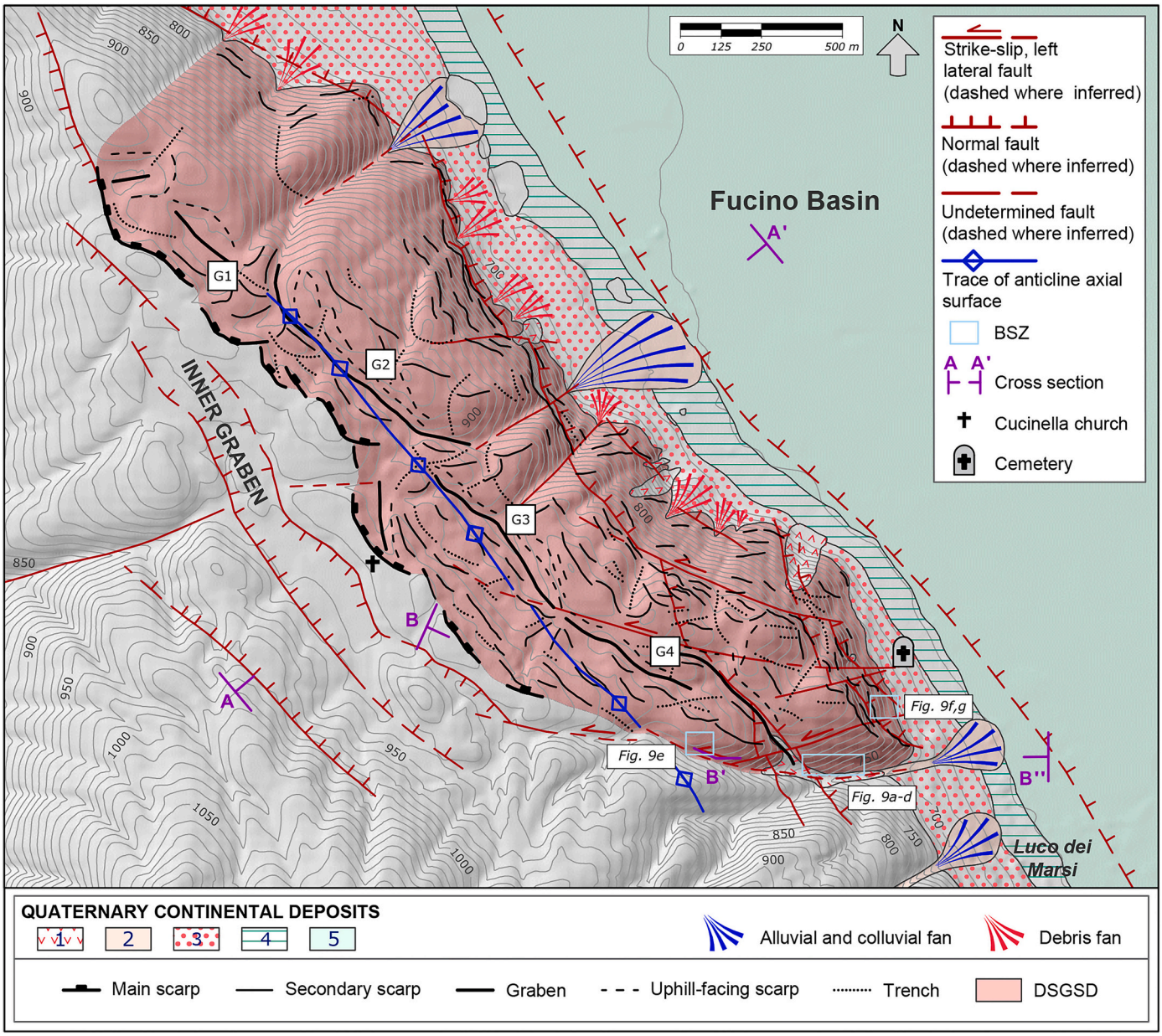

Fig. 7. Inventory map of geomorphological features ascribable to the Luco dei Marsi DSGSD and location of the BSZ outcrops along the southern edge. Structural and tectonic elements from Fig. 1b are reported. Legend: Quaternary deposits: 1) landslides; 2) residual clay deposits; 3) talus slope deposits; 4) eluvial-colluvial deposits; and 5) alluvial and lacustrine deposits of the Fucino Basin. G1–G4 = gravitational grabens.

5.1. *Short-term activity of the Luco dei Marsi DSGSD*

Despite the thick vegetation cover, the DInSAR monitoring technique was helpful in investigating the present activity and short-term kinematics of the gravitational deformation, providing spatial information on ground movements in the last thirty years. Displacement rate maps (Figs. 10a–d, 12a, b) differentiate a central-northern sector with low deformation rates from a southern area, near the BSZ, with higher values. Cumulative time series were derived combining ERS1/2, ENVISAT, and COSMO-SkyMed SENTINEL 1 data (Fig. 11c, d), thus covering the 1993–2019 period, and indicating a deformation rate of approximately 1.5 mm/y in the southern sector of the DSGSD. Deformation rates estimated over a shorter time interval (2011–2019) indicate even higher values, approximately 6.0 mm/y, along the main rear scarp and in the BSZ zone (Fig. 11e, f); these values could be due to the short time window or an increased deformation rate along the DSGSD boundary surfaces. However, as demonstrated by the monitoring data, the Luco dei Marsi DSGSD appears active and still in evolution, with a deformation rate on the order of a few millimetres/year.

5.2. *Long-term activity of the Luco dei Marsi DSGSD: geomorphological evidence*

The lifespan of the gravitational deformation over a longer time interval (>10^2 y) can be inferred by geomorphological evidence that reveals significant clues once contextualized to the Pliocene-Quaternary evolution of the Fucino Basin. Bosi et al. (1996) recognized two orders of regional paleosurfaces on both sides of the continental basin at 1100 ± 50 and 950 ± 50 m a.s.l., respectively. In particular, the latter is ascribed to an Early-Middle Pleistocene phase of subaerial erosion in the embryonic continental environment featuring the Apennine landscape at that time (Galadini et al., 2003). The top flat surfaces identified in this

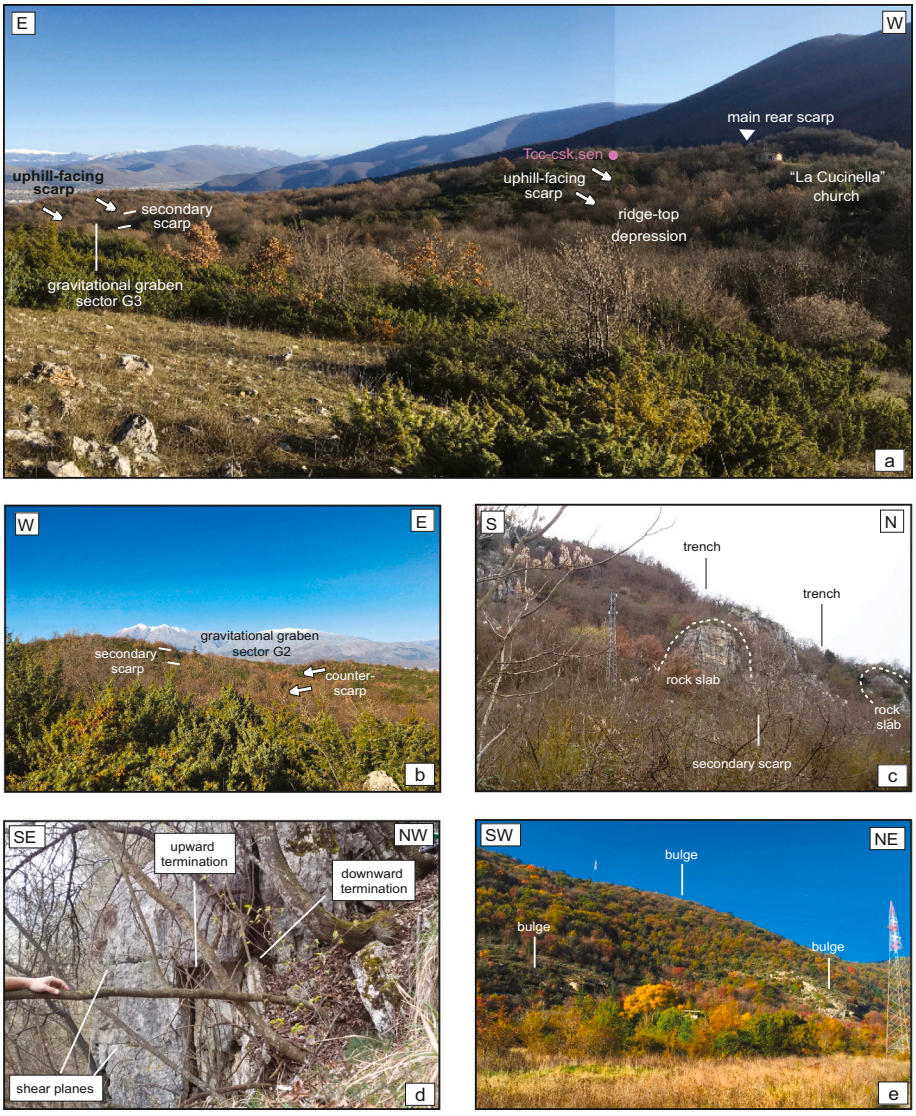

Fig. 8. Gravity-driven structures. a) Panoramic view of the uppermost sector of the Luco dei Marsi DSGSD. The main geomorphic features are reported (Tcc-csk and Tcc-sen indicate the positions of targets in the interferometric analysis); b) the gravitational graben sector G2; c) rock slabs separated by trenches on the eastern edge of the slope; d) mesoscale deformation features (extensional fractures and shear planes); and e) bulging at the slope base.

work (Figs. 5, 6a, b) are distributed from 830 to 1025 m a.s.l. (with a general dip of 2–6° towards the Fucino Basin) and can be classified into six classes (PS1–PS6) on a morphological basis (Fig. 13). Indeed, classes PS3 and partly PS4 are in the same elevation range of the regional feature (950 ± 50 m a.s.l.) described by Bosi et al. (1996).

Most paleosurfaces observed within the Luco dei Marsi DSGSD are dismembered or interrupted by gravitational features (scarps, uphill-facing scarps, and trenches) and reduced to very small flat areas compared to surfaces outside the limits (Figs. 5, 13). Vertical offsets between adjacent paleosurfaces within the DSGSD can be up to several metres, as demonstrated by the dislocation of PS3 with respect to PS4. All this evidence suggests a specific role of the gravitational deformation process in the Quaternary evolution of the ridge.

5.3. *Quaternary evolution of the Luco dei Marsi DSGSD: a conceptual model*

Geological and paleoseismological information from previous studies (Giraudi, 1988; Bosi et al., 1995, 1996; Galadini and Galli, 1999; Cavinato et al., 2002; Di Naccio et al., 2020) was integrated with the geomorphological evidence from this work to obtain a multiple-step, conceptual model unravelling the possible relationship between the DSGSD and the Quaternary evolution of the western edge of the Fucino Basin. The model attempts to summarize the main erosional, depositional, and tectonic events that affected the Luco dei Marsi slope between the Early-Middle Pleistocene and the historical epoch (Fig. 14).

Few assumptions and simplifications were made, the main ones concerning the elevation values, which are kept only as a dimensional reference in single steps. Indeed, Quaternary topography in the central Apennine has been controlled by regional uplift since the end of the Early Pleistocene (e.g., D'Agostino et al., 2001) or even earlier (Galadini et al., 2003); a geodynamic process that is difficult to ponder at the local scale. Second, each of the four steps illustrates the conditions hypothesized at the end of the main erosional cycles. Finally, a minor uncertainty concerns the inner graben (Figs. 1b, 4d), for which no reliable data are available. Considering its well-developed structure and dimensions (2.0 km in length and 0.25 km in width), this morphotectonic depression is hypothetically dated back to the first tectonic phase that occurred in the area during the late Pliocene (Cavinato and De Celles, 1999).

The first step of the model refers to the Early-Middle Pleistocene transition (Fig. 14a). The landscape experienced subaerial erosion after

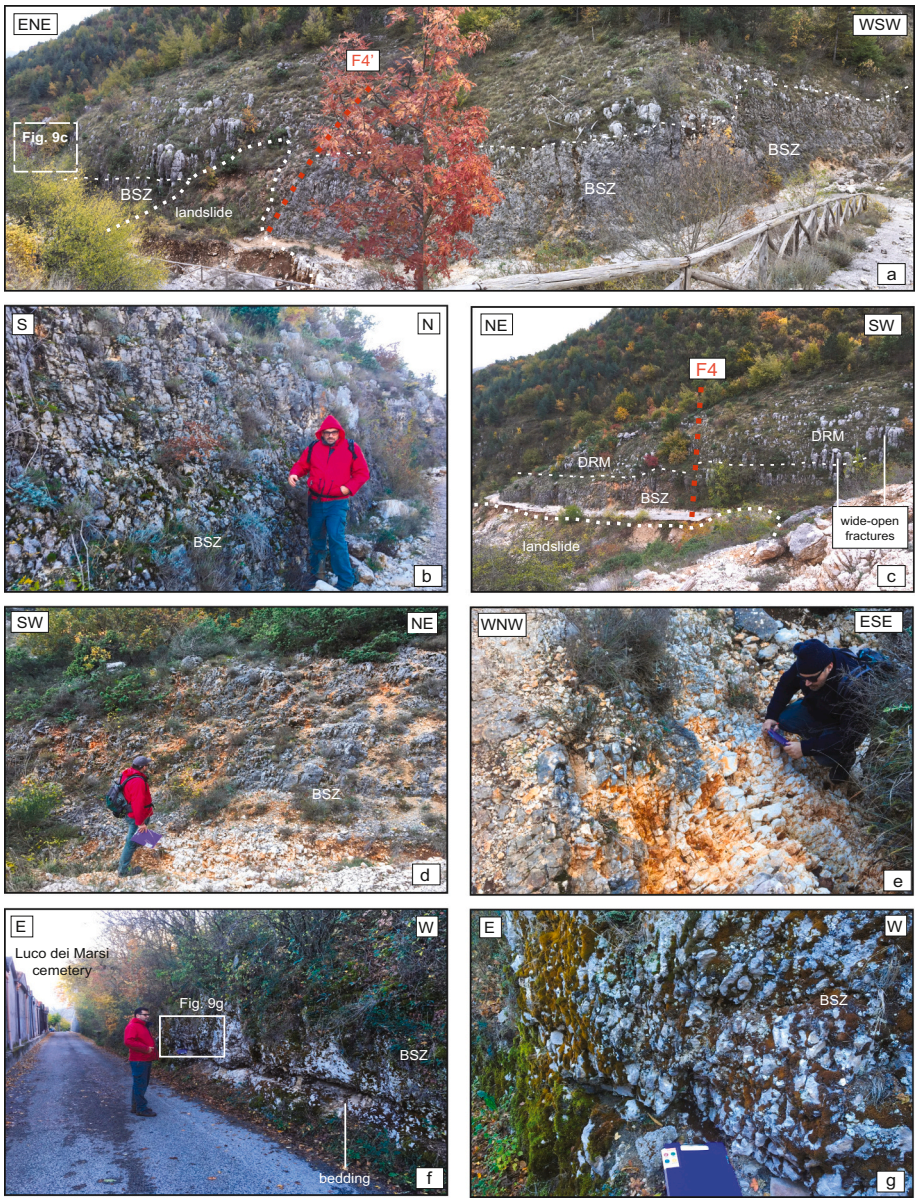

Fig. 9. The basal shear zone (BSZ): a) outcrop within the southern gully. F4′ is a NNW-SSE-oriented normal fault that displaces the BSZ boundaries; b) cataclastic texture of the highly fragmented rock mass; c) deforming rock mass (DRM) overlying the BSZ and involved in the Luco dei Marsi DSGSD; d) evidence of karst dissolution leaving residual, red clays within the BSZ; e) outcrop of the BSZ in the uppermost part of the slope and f), g) along the base of the slope, near the cemetery. (For interpretation of the references to color in this figure legend, the reader is referred to the web version of this article.)

the deposition of Upper Pliocene-Lower Pleistocene alluvial and lacustrine sediments. The basal sequence (Aielli complex *Auctt.*, late Pliocene) of the Fucino Basin, found only along the eastern border, contains siliciclastic breccias proving the dismantling of the Miocene flysch originally covering the carbonate units. The following Lower Pleistocene deposits, derived from the erosion of carbonate sequences only (Cupoli complex *Auctt.*), are limited upwards by the regional erosion surface currently found at 950 ± 50 m a.s.l. (Bosi et al., 1995, 1996) and identified with PS3 and PS4 in this work. Fault activity at this stage was confined on the northern and eastern edges of the basin (Cavinato et al., 2002). Accordingly, the conceptual model represents the study area as a low-gradient continental slope corresponding to a wide erosional surface.

After the partial erosion of the Lower Pleistocene deposits, renewed subsidence gave rise to the sedimentation of (late) middle Pleistocene lacustrine, fluvial, and deltaic deposits (Fig. 14b). Again, basin extension and fault activity were largely concentrated along the northeastern edge of the basin (Cavinato et al., 2002). Even this depositional cycle was followed by an erosional stage; Bosi et al. (1995) evidenced a subhorizontal surface at approximately 800–850 m a.s.l. on the top of the Middle Pleistocene sequence (Pervole Formation *Auctt.*), also carved in the carbonate ridges surrounding the basin (Bosi et al., 1996). Indeed, the elevation of the lowest paleosurface recognized in this work (PS6) lies in a similar range, between 845 and 830 m a.s.l. (Figs. 3a, 13). At this stage, depositional and erosional processes in the Luco dei Marsi area were probably accompanied by early tectonic activity along normal faults F1–F4, which dissected the carbonate bedrock, thus preserving the middle Miocene deposits (mM in Figs. 3a, 4c) by aerial erosion in the hanging wall blocks (Fig. 14b). However, the absence of a thick depositional wedge along the piedmont junction zone suggests a low cumulative displacement at the end of the middle Pleistocene and still a low-energy relief.

The third step of the evolutionary model illustrates the Luco dei Marsi slope at the end of the late Pleistocene (Fig. 14c). The local palaeomorphology was characterized by a surface of lake abrasion formed between 30 and 16 ky B.P. as recognized by Giraudi (1988) along the base of Mt. Salviano ridge at an elevation of approximately 700 m a.s.l. In this work, faint evidence of this surface was found along the edge of the slope (see Section B-B′ in Fig. 3b). According to Cavinato et al. (2002), starting from the late Pleistocene, the western edge of the

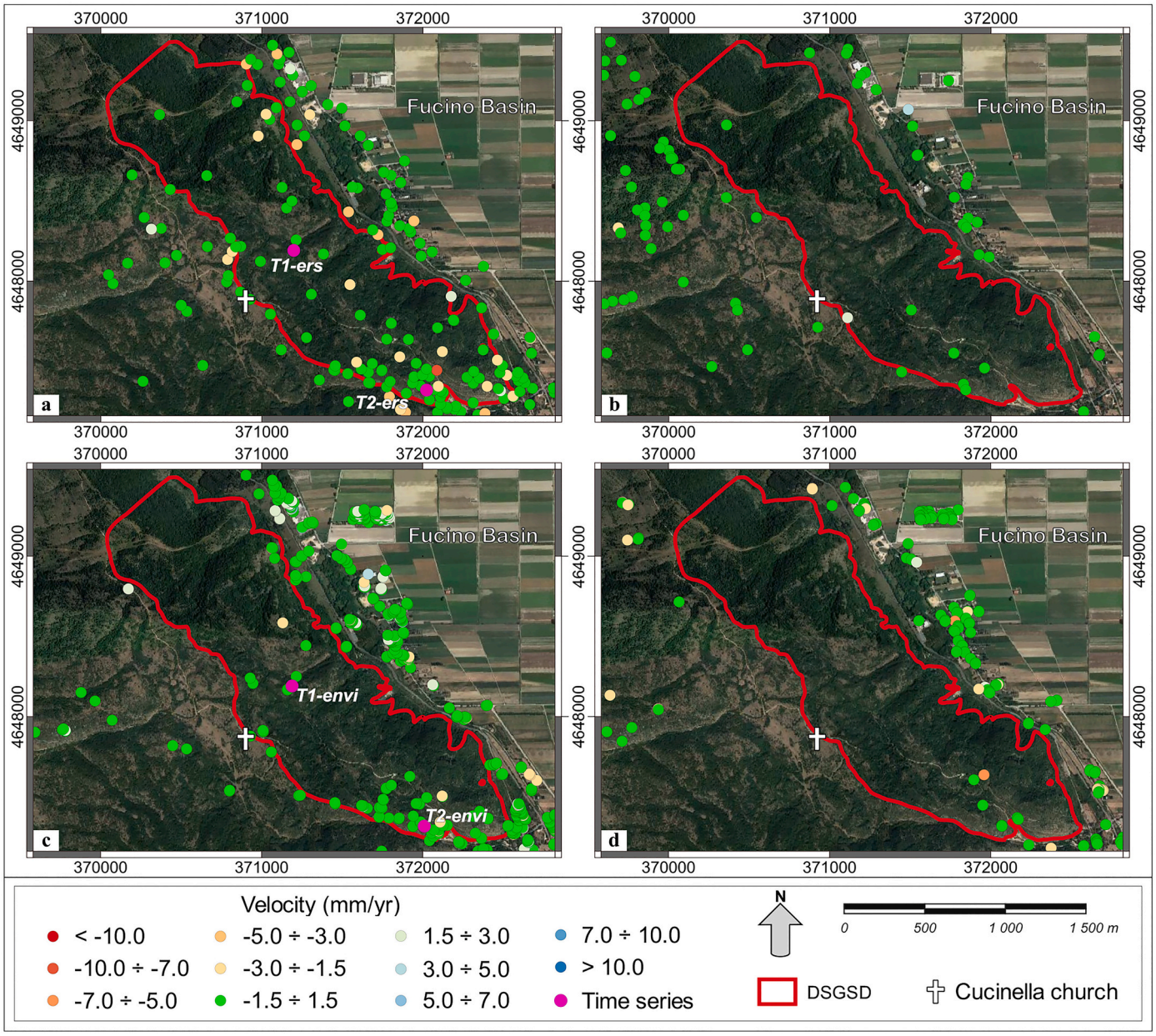

Fig. 10. Mean displacement rate maps for ERS1/2 (1993–2000 time span) and ENVISAT (2002–2010 time span) datasets: a) ERS and c) ENVISAT ascending; and b) ERS and d) ENVISAT descending.

Fucino Basin began to be affected by significant normal faulting: the model assumes faults F1–F4 (Figs. 1b, 3a, b) to be responsible for the large, cumulative vertical displacement accumulated during the late Pleistocene.

Finally, the last step shows a situation very close to the present day (Fig. 14d). Still following Giraudi (1988), an accumulation surface of lacustrine deposits lies along the western edge of the Fucino Basin at approximately 660–665 m a.s.l. and dates back to an interval between the late Iron Age (XI sec. B.C.) and the Roman period (VI century B.C.). This surface was recognized in the study area along the piedmont junction zone (Fig. 3a, b). Regarding the recent tectonic activity, paleoseismological evidence suggests a basinward migration of normal faulting with the activation of the LMF in the Holocene. Galadini and Galli (1999) estimated a very low displacement (0.1–0.2 m) accumulated between a seismic event in the I-II cen. A.D. and the 1915 Fucino earthquake. Recent studies for microzonation purposes (Di Naccio et al., 2020) observed a vertical downthrow for the carbonate bedrock in the LMF hanging wall lower than 100 m, with the top of the carbonates found at approximately 550 m a.s.l. This depth of the carbonate bedrock along the western margin of the Fucino Basin and the low amount of vertical displacement along the LMF are confirmed from the interpretation of seismic lines crossing the Luco dei Marsi-Mt. Salviano ridge (Cavinato et al., 2002; Patacca et al., 2008; Di Luzio et al., 2009).

The conceptual model therefore identifies the latest Pleistocene as the moment in which extensional tectonics along longitudinal faults F1–F4 determined the lateral unconfinement of the Luco dei Marsi rock slope. The gravitational deformation then originated between 0.126 and 0.018 My. A more precise time frame is difficult to define. However, some consideration can be made by combining evidence from palaeosurface dislocation and short-term deformation rates revealed by DInSAR analysis. The main paleosurface recognized in the Luco dei Marsi ridge (class PS3 in Fig. 13) inside the DSGSD is dismembered in flat areas with low extension. The vertical downthrow among areas outside (PS3) and within the DSGSD (PS3–4) ranges between 55 and 65

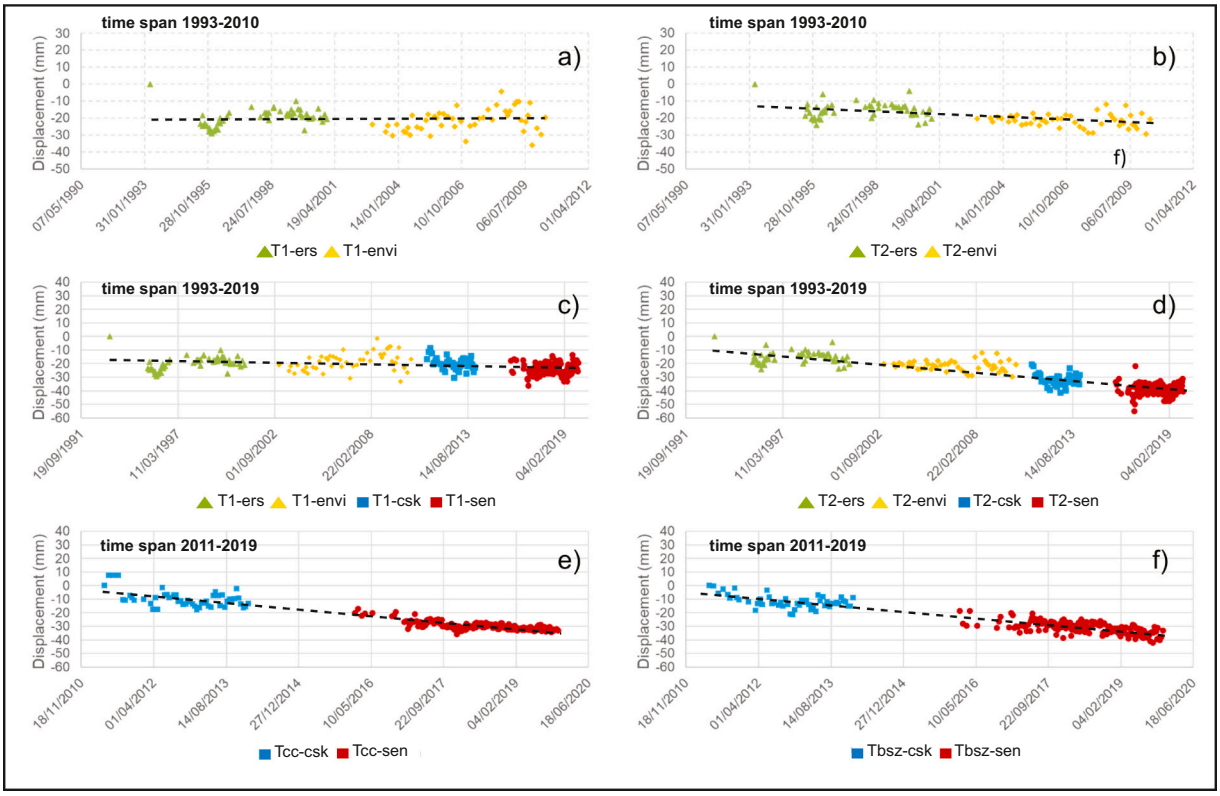

Fig. 11. Cumulative time series of deformation (1993–2010 time span) for a) T1-ers and T1-envi targets; and b) T2-ers and T2-envi targets (see Fig. 10a, c for location). Cumulative time series of deformation (1993–2019 time span) for c) T1-ers, T1-envi, T1-csk, and T1-sen targets; and d) T2-ers, T2-envi, T2-csk, and T2-sen targets (see Figs. 10a, c, 12a, and b for location). Cumulative time series of deformation (2011–2019 time span) for e) targets Tcc-csk and Tcc-sen and f) targets Tbsz-csk and Tbsz-sen (Fig. 12a, b for location). Legend: ers = ERS; envi = ENVISAT; csk = COSMO-SkyMed; and sen = SENTINEL 1 dataset.

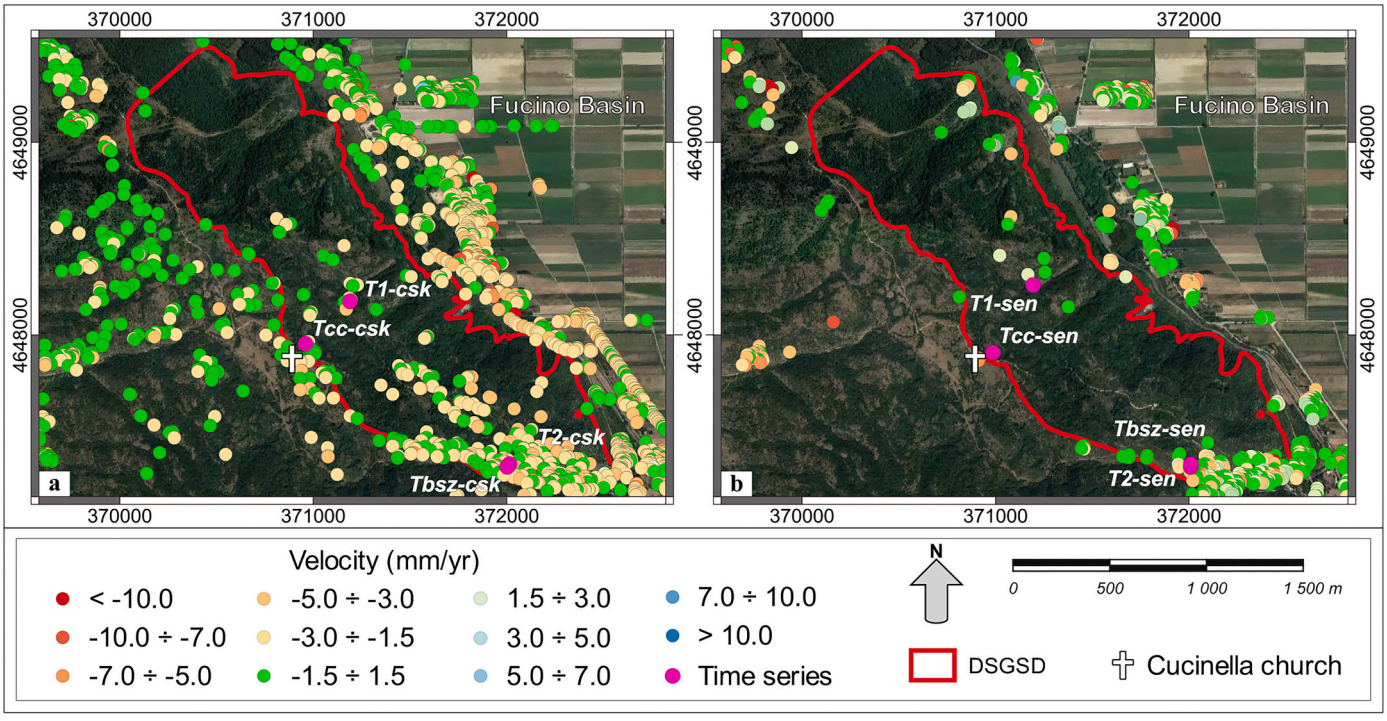

Fig. 12. a) Mean displacement rate maps for COSMO-SkyMed (2011–2014 time span), descending images; and b) mean displacement rate maps for SENTINEL-1 (2016–2019 time span), descending images.

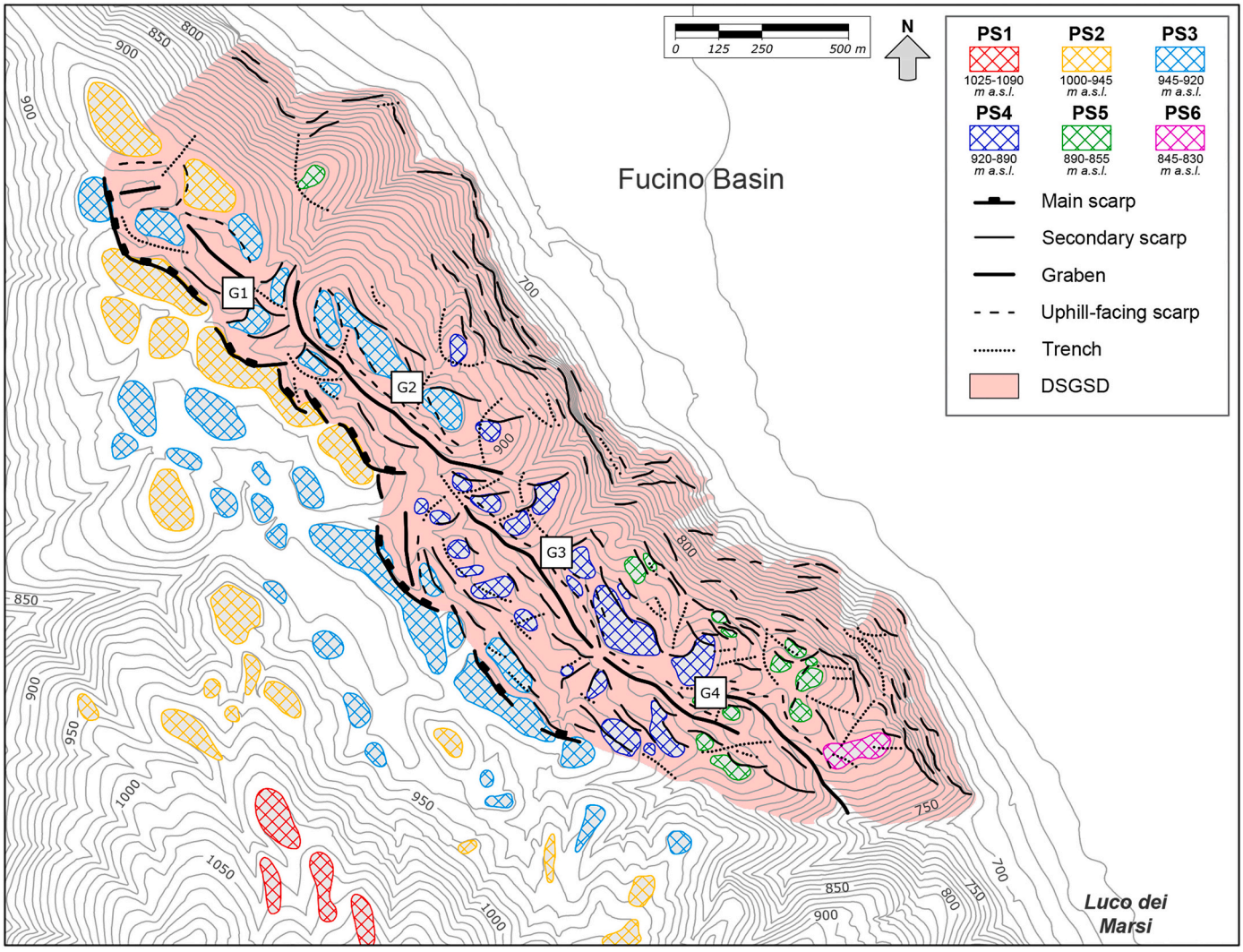

Fig. 13. Classification map of paleosurfaces in the study area, distinguished on the basis of their elevation.

m. Such cumulative dislocation is largely attributed to gravitational deformation since it cannot be explained over distances of tens to hundreds of metres considering only the moderate slope of the original palaeosurface. Then, if a stationary DSGSD process is invoked and the deformation rate shown over the last thirty years (1.5 mm/y) for the southern sectors (Fig. 11d) is considered entirely along the vertical dimension, the dislocation of paleosurfaces would have been realized since 43,000–37,000 yr. B.P. during the latest Pleistocene. This time frame becomes overestimated if part of the displacement is assigned to the horizontal component (as it is plausible in relation to the kinematic reconstruction of the deformational process, characterized by a low-angle BSZ). Other studies in the Apennine belt revealed a post-Early Pleistocene age of DSGSD activation (Bianchi Fasani et al., 2011; Gori et al., 2014).

5.4. *Deformation style and relationship with inherited structural features. The meaning of the BSZ*

The DSGSD affecting the Luco dei Marsi ridge is characterized, on the upper part of the slope, by a main longitudinal scarp, several secondary downhill- and uphill-facing scarps, grabens, and trenches. These morphostructures draw a complex network of discontinuous, short (from tens to a few hundreds of metres long), curvilinear or arc-shaped features that can be easily distinguished from the continuous (up to more than 2 km long), rectilinear tectonic elements bordering the inner graben to the west and gathering along the eastern edge of the slope (Fig. 7). Here, intense gravity-driven deformation is indicated by the presence of isolated rock slabs (Fig. 8c) and mesoscale structures (Fig. 8d), whereas bulging is observed in the lower slope sectors (Fig. 8e).

The Luco dei Marsi DSGSD has been developing along the eastern limb of a wide anticline with a NW-SE-oriented axis. The control of inherited structures in the DSGSD appears similar to other case histories observed in the central Apennines (Di Luzio et al., 2004a; Scarascia Mugnozza et al., 2006; Esposito et al., 2007, 2021; Moro et al., 2012; Gori et al., 2014; Bianchi Fasani et al., 2014; Della Seta et al., 2017), and a partial overlap between tectonic and gravity-driven features is evident. This can be observed in the 3D-geological sketch shown in Fig. 15a: i) the gravitational grabens (G1–G4) are located corresponding to the fold axial culmination zone, and their formation was likely favoured by tensile strain and pervasive brittle deformation in the extrados area of the anticline (Dramis and Sorriso-Valvo, 1994); ii) the peripheral bulging (Fig. 8e) is superimposed on a knick zone in the fold forelimb, where the bedding dip increases from 10–18° to 20–25° (see also Fig. 3a, b); iii) the rock slabs on the eastern edge of the slope (Figs. 4a, 8c) are elongated in the same direction as longitudinal faults F1–F4; and iv) finally, the boundary of the DSGSD is better outlined in the southern zones of the Luco dei Marsi ridge, where WNW-ESE-oriented strike-slip faults (T1–T5) control the slope morphology (Fig. 7).

However, some geomorphic features of the DSGSD seem to be

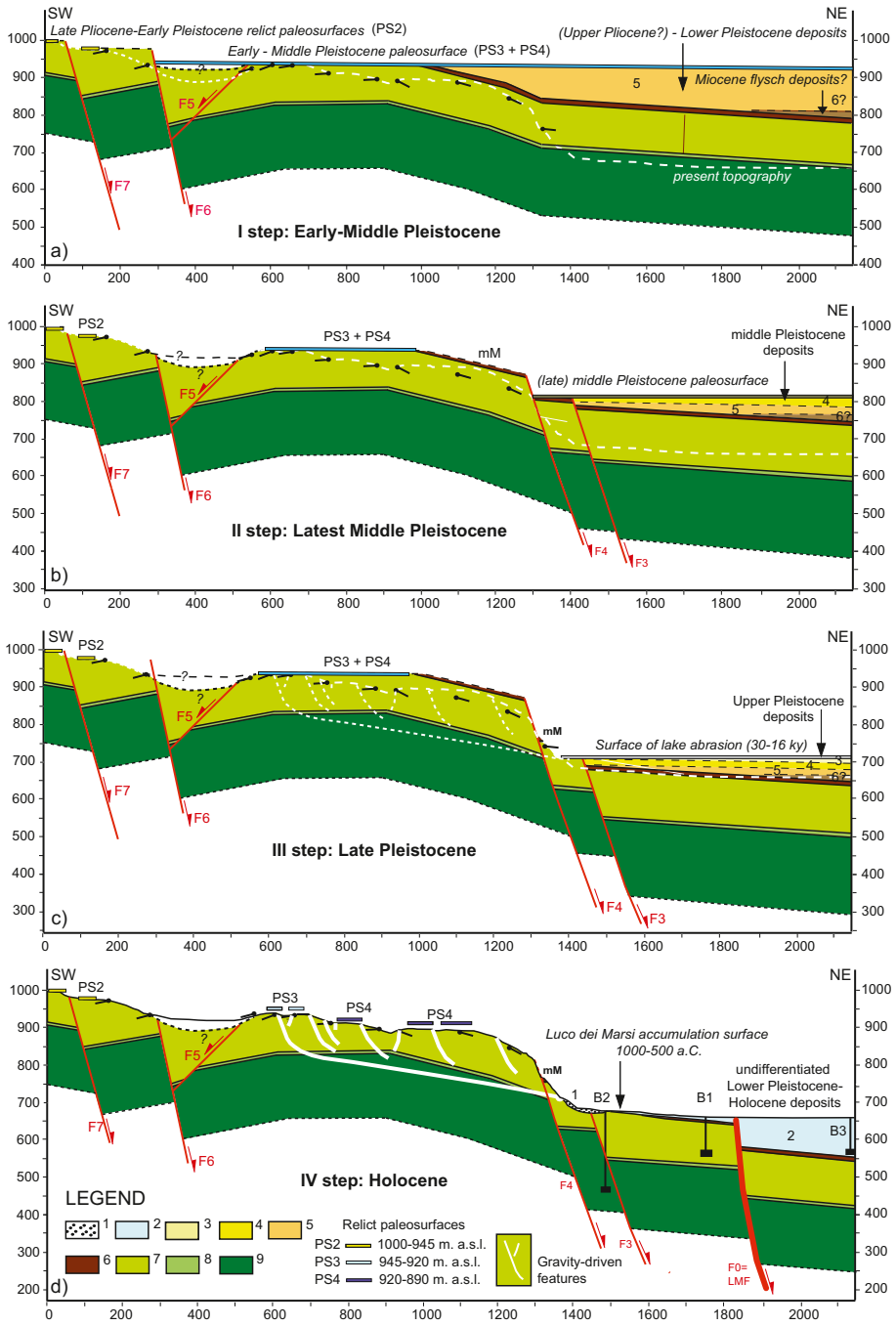

Fig. 14. Multiple-step, conceptual model of the Quaternary morphotectonic evolution of the Luco dei Marsi ridge and the Fucino Basin western edge. a): subaerial erosion following deposition of Upper Pliocene-Lower Pleistocene alluvial and lacustrine deposits; b) renewed erosion after sedimentation of middle Pleistocene lacustrine, fluvial, and deltaic deposits. Early tectonic activity; c) late Pleistocene lacustrine environment. The intense tectonic activity along the edge of the slope activated the DSGSD process; d) basinward migration of tectonic activity along the LMF, full development of the DSGSD. Legend: 1) talus deposits; 2) undifferentiated Quaternary deposits of the Fucino Basin; 3), 4), 5) Upper, middle, and Lower Pleistocene alluvial and lacustrine deposits; 6) Miocene flysch deposits; and 7), 8), 9) Upper, middle-and Lower Cretaceous limestone.

independent from the main faults inherited by the Neogene-Quaternary tectonics. The main scarp lies a few hundred metres outside the axial zone in the fold backlimb (Fig. 15a). Several orders of secondary scarps and uphill-facing scarps with a longitudinal trend were found far from main faults F1–F7 (Fig. 7). Additionally, trenches and other NE-SW- to E-W-oriented features did not overlap former tectonic elements and separate sectors with different deformation rates (Fig. 11a–d). Finally, the high-angle discontinuities in the DRM immediately above the BSZ (Fig. 9b) may be due to slope debutressing (although inherited strain on the fold extrados may have played a role). According to (Hutchinson, 1988), the high degree of internal deformation and the several orders of uphill-facing elements can be considered evidence for a (listric?) compound sagging (sackung) kinematic.

The relationship between inherited tectonic features and gravitational elements becomes more puzzling when considering the position and trend of the BSZ. The Luco dei Marsi DSGSD represents a singularity with respect to the majority of cases in the central Apennines where many DSGSDs developed along the backlimbs of thrust folds (Fig. 15b), partly reactivating west-dipping thrust surfaces (Nijman, 1971; Moro et al., 2012; Gori et al., 2014; Esposito et al., 2021) or normal to transcurrent, high-angle faults (Di Luzio et al., 2004a; Esposito et al., 2013, 2014; Bianchi Fasani et al., 2014), locally defined as gravitational collapse faults (Patacca et al., 2008). In contrast, in our case study, the BSZ developed along the forelimb section of a thrust fold (Fig. 15a, b) with moderate brittle deformation along few, longitudinal faults showing negligible downthrow (Figs. 4c and 9a, b). Undoubtedly, the BSZ is a newly generated feature since no pre-existing structural element was reused. At least, passive control of bedding anisotropies

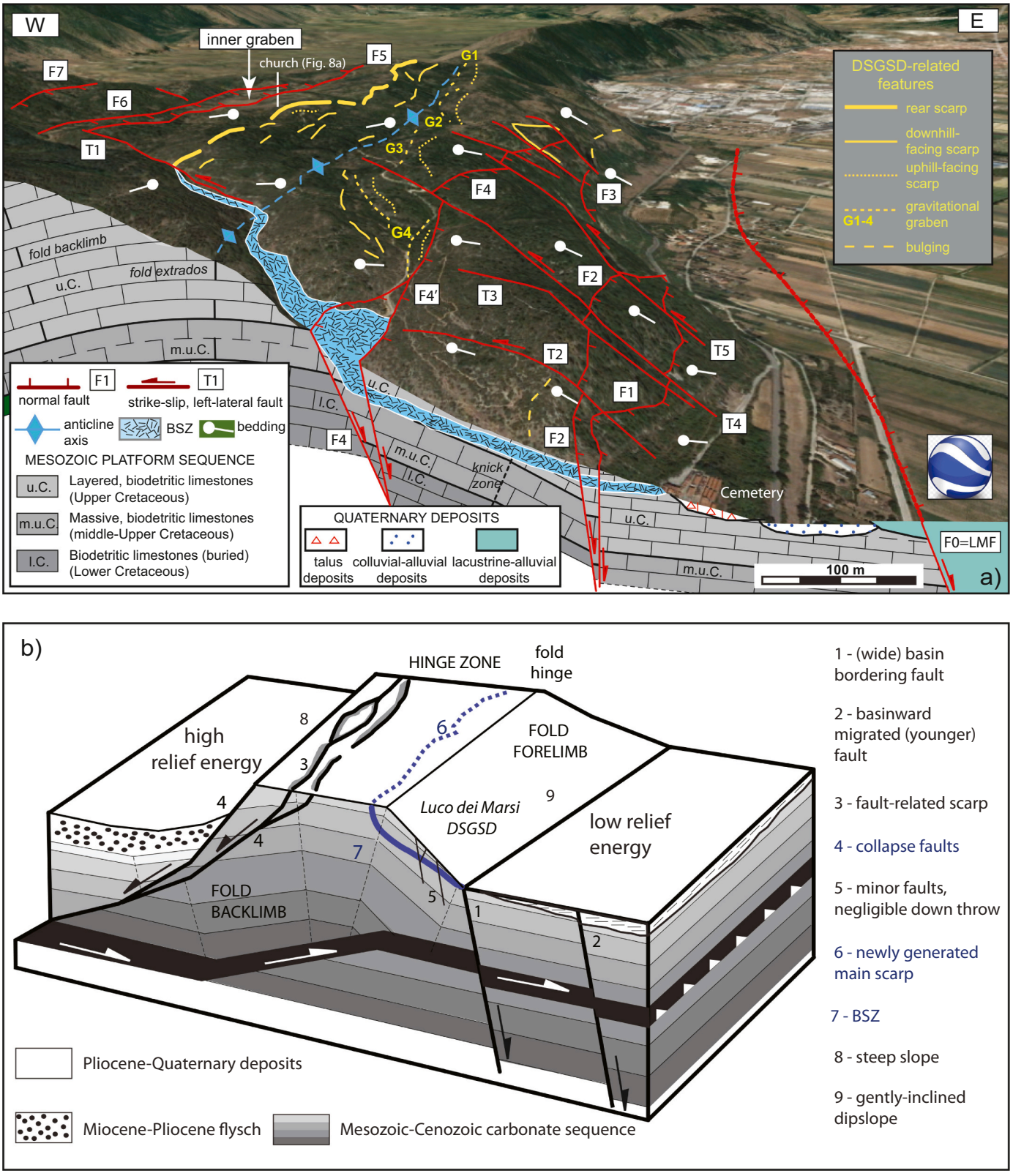

Fig. 15. a) 3D-geological sketch showing the fold structure, main faults, extension and geometry of the Luco dei Marsi DSGSD, including the BSZ. Legend: C.C. = La Cucinella Church; F1–F6 = normal faults; T1–T5 = transcurrent faults; and F0 = LMF = Luco dei Marsi Fault. Google Earth Image: Landsat/Copernicus, 10/10/2019; and b) simplified block diagram of a fault-bend fold structure later affected by DSGSDs in the backlimb and forelimb sectors.

(Discenza et al., 2020) can be hypothesized since the BSZ developed following the bedding attitude and the lithological contrast between Upper Cretaceous well-layered, jointed limestone and middle-Upper Cretaceous massive limestone (Fig. 15a). The BSZ is an anomaly in the local structural framework and can be considered a slope-tectonic related feature.

Although the structural control on DSGSD onset and development has been largely documented in the Apennine belt, the discovery of the Luco dei Marsi BSZ demonstrates how the Neogene inheritance is not strictly necessary for the development of slope-scale gravitational features. This evidence can be extrapolated to other DSGSD cases worldwide.

Finally, the trend of the BSZ at depth in the central and northern sectors is an unsolved issue. In Fig. 3a, we adopt a conservative approach, and the BSZ is drawn within the same elevation range as the southern gully. The breccia level locally seems to be displaced by longitudinal normal faults, although with a reduced downthrow (Fig. 9a, b). However, it is not clear if the BSZ geometry at depth is also influenced by these tectonic discontinuities, or it depends exclusively on the compound configuration of the DSGSD. In this last case, single outcrops observed within the deeply incised rock gully (Fig. 9a–d) and near the cemetery (Fig. 9f, g) could be connected by a subplanar deformational zone (Fig. 15). Further studies, including geophysical prospecting and numerical modelling, will be necessary to unravel this issue.

6. Conclusions

The Luco dei Marsi DSGSD is a new case of slow, slope-scale deformation observed in the axial zone of the central Apennines. Gravitational deformation developed in a carbonate ridge featuring a fault-bounded anticline along the western edge of the Fucino Basin, the largest Quaternary tectonic depression of the belt. The inherited (Neogene) fold structure and main Quaternary fault systems have influenced the extension and boundary conditions of the DSGSD. Nevertheless, some geomorphic features on the hilltop sector (main and secondary scarps, uphill-facing scarps and trenches) did not overlap with former tectonic elements. This extensive internal deformation and the pattern of gravity-driven features are considered a clue for a compound sagging configuration. In this work, much field evidence of a well-exposed basal shear zone is presented. This feature has been recognized in DSGSD phenomena worldwide, but no similar case has been reported thus far for the central Apennines. The BSZ appears in the field as a damaged rock zone, several metres thick and made of cataclastic calcareous breccia with a fine matrix. With a subhorizontal to gently inclined geometric attitude, the BSZ can be observed for several tens of metres and is considered a newly generated feature, depending on slope tectonic processes.

Beyond this aspect, the recent activity of the Luco dei Marsi DSGSD was investigated by DInSAR datasets covering the 1997–2019 time span. Although with different details and resolutions, the ERS1/2, ENVISAT, COSMO-SkyMed and SENTINEL 1 datasets show a deformation rate of approximately 1.5 mm/y for the last three decades in the southern sector, near the BSZ. In addition, the long lifespan activity of the DSGSD was inferred through the reconstruction of a multiple-step conceptual model illustrating the main geological events controlling the morpho-tectonic evolution of the local slope-to-basin system from the Early-Middle Pleistocene to the historical period.

Latest Pleistocene fault activity was inferred as the main cause for slope lateral unconfinement driving the onset of the DSGSD and the development of the BSZ. This age estimate agrees with a temporal extrapolation of short-term deformation rates revealed by DInSAR analysis and the magnitude of vertical dissection of relict paleosurfaces.

Further studies will be necessary to outline the physical and geomechanical properties of the BSZ and its position at depth. Such insights will possibly unravel the kinematic and dynamic role of the BSZ, which represents an element of particular importance for many DSGSDs.

Declaration of competing interest

The authors declare that they have no known competing financial interests or personal relationships that could have appeared to influence the work reported in this paper.

Acknowledgements

The authors want to thank Cavinato G.P., Giaccio, B. and Messina, P. (CNR-IGAG) for the useful discussion on geology of the Fucino Basin and two anonymous reviewers whose contribution improved the quality of the paper. This work was financially supported by the research project “Integrated analysis and hazard-oriented modelling of large-scale slope instabilities featured by Mass Rock Creep” - prot. RG11916B88FA477F (PI Prof. Carlo Esposito) fund by “Sapienza” University of Rome. The writing of this paper began in the first months of winter 2020, when the Covid-19 emergency hit Italy very hard. Our thoughts go to all those people in our country and elsewhere who in those days did a much more important job than ours as doctors, nurses, health assistants, and to fellow researchers in the medical sciences for their invaluable and unremitting work. up to present days.

References

Agliardi, F., Crosta, G.B., Zanchi, A., 2001. Structural constraints on deep-seated slope deformation kinematics. Eng. Geol. 59, 83–102. https://doi.org/10.1016/S0013-7952(00)00066-1.

Agliardi, F., Crosta, G.B., Frattini, P., 2012. Slow rock-slope deformation. In: Clague, J.J., Stead, D. (Eds.), Landslides: Types, Mechanisms and Modeling. Cambridge University Press, Cambridge, pp. 207–221. https://doi.org/10.1017/CBO9780511740367.019.

Agliardi, F., Riva, F., Barbarano, M., Zanchetta, S., Scotti, R., Zanchi, A., 2019. Effects of tectonic structures and long-term seismicity on paraglacial giant slope deformations: Piz Dora (Switzerland). Eng. Geol. 263, 105353 https://doi.org/10.1016/j.enggeo.2019.105353.

Ambrosi, C., Crosta, G.B., 2006. Large sackung along major tectonic features in the Central Italian Alps. Eng. Geol. 83, 183–200. https://doi.org/10.1016/j.enggeo.2005.06.031.

Ambrosi, C., Crosta, G.B., 2011. Valley shape influence on deformation mechanisms of rock slopes. Geol. Soc. London Spec. Publ. 351, 215–233. https://doi.org/10.1144/SP351.12.

Antonielli, B., Mazzanti, P., Rocca, A., Bozzano, F., Dei Cas, L., 2019. A-DInSAR performance for updating landslide inventory in mountain areas: an example from Lombardy Region (Italy). Geosciences 9 (9), 364. https://doi.org/10.3390/geosciences9090364.

Barla, G., Antolini, F., Barla, M., Mensi, E., Piovano, G., 2010. Monitoring the Beauregard landslide (Aosta Valley; Italy) using advances and conventional techniques. Eng. Geol. 116, 218–235. https://doi.org/10.1016/j.enggeo.2010.09.004.

Bartolini, C., D'Agostino, N., Dramis, F., 2003. Topography, exhumation and drainage network evolution of the Apennines. Episodes 26, 212–216. https://doi.org/10.18814/epiiugs/2003/v26i3/010.

Bianchi Fasani, G., Di Luzio, E., Esposito, C., Martino, S., Scarascia Mugnozza, G., 2011. Numerical modeling of Plio-Quaternary slope evolution based on geological constraints: a case study from the Caramanico Valley (central Apennines, Italy). Geol. Soc. London Spec. Publ. 351, 201–214. https://doi.org/10.1144/SP351.11.

Bianchi Fasani, G., Di Luzio, E., Esposito, C., Evans, S.G., Scarascia Mugnozza, G., 2014. Quaternary, catastrophic rock avalanches in the Central Apennines (Italy): relationships with inherited tectonic features, gravity-driven deformations, and the geodynamic frame. Geomorphology 211, 22–42. https://doi.org/10.1016/j.geomorph.2013.12.027.

Bonzanigo, L., Eberhardt, E., Loew, S., 2007. Long-term investigation of a deep-seated creeping landslide in crystalline rock. Part I. Geological and hydromechanical factors controlling the Campo Vallemaggia landslide. Can. Geotech. J. 44 (10), 1157–1180. https://doi.org/10.1139/T07-043.

Bosi, C., Galadini, F., Messina, P., 1995. Stratigrafia plio-pleistocenica della Conca del Fucino. Il Quaternario 8, 83–94.

Bosi, C., Caiazzo, C., Cinque, A., Messina, P., 1996. Le superfici relitte della regione fucense (Appennino centrale) ed il loro possibile significato nella ricostruzione della evoluzione geologica. Il Quaternario 9, 381–386.

Bovis, M.J., 1982. Uphill-facing (antislope) scarps in the Coast Mountains, southwest British Coulumbia. Geol. Soc. Am. Bull. 93, 804–812.

Bozzano, F., Mazzanti, P., Perissin, D., Rocca, A., De Pari, P., Discenza, M.E., 2017. Basin scale assessment of landslides geomorphological setting by advanced InSAR analysis. Remote Sens. 9 (3), 267. https://doi.org/10.3390/rs9030267.

Bozzano, F., Esposito, C., Mazzanti, P., Patti, M., Scancella, S., 2018. Imaging multi-age construction settlement behaviour by advanced SAR interferometry. Remote Sens. 10 (7), 1137. https://doi.org/10.3390/rs10071137.

Cappadonia, C., Confuorto, P., Sepe, C., Di Martire, D., 2019. Preliminary results of a geomorphological and DInSAR characterization of a recently identified Deep-Seated

Gravitational Slope Deformation in Sicily (Southern Italy). Rend. Online Soc. Geol. Ital. 49, 149–156. https://doi.org/10.3301/ROL.2019.65.
Cavinato, G.P., De Celles, P.G., 1999. Extensional basins in the tectonically bimodal central Apennine fold-thrust belt, Italy: response to corner flow above a subducting slab in retrograde motion. Geology 27 (10), 955–958. https://doi.org/10.1130/0091-7613(1999)027<0955:EBITTB>2.3.CO;2.
Cavinato, G.P., Carusi, C., Dall'Asta, M., Miccadei, E., Piacentini, T., 2002. Sedimentary and tectonic evolution of Plio-Pleistocene alluvial and lacustrine deposits of Fucino Basin (central Italy). Sediment. Geol. 148, 29–59. https://doi.org/10.1016/S0037-0738(01)00209-3.
Chigira, M., 1992. Long-term gravitational deformation of rocks by mass rock creep. Eng. Geol. 32, 157–184.
Cigna, F., Bateson, L.B., Jordan, C.J., Dashwood, C., 2014. Simulating SAR geometric distortions and predicting Persistent Scatterer densities for ERS-1/2 and ENVISAT C-band SAR and InSAR applications: Nationwide feasibility assessment to monitor the landmass of Great Britain with SAR imagery. Remote Sens. Environ. 152, 441–466. https://doi.org/10.1016/j.rse.2014.06.025.
Cinti, G., Donati, A., Fumanti, F., Scarascia-Mugnozza, G., 2001. La grande frana di Mt. Arezzo (Abruzzo). Mem. Soc. Geol. It. 56, 41–50.
Cosentino, D., Cipollari, P., Marsili, P., Scrocca, D., 2010. Geology of the central Apennines: a regional review. In: Beltrando, M., Peccerillo, A., Mattei, M., Ponticelli, S., Dogliosi, C. (Eds.), The Geology of Italy, Journal of the Virtual Explorer, Electronic edition, 36. https://doi.org/10.3809/jvirtex.2010.00223. paper 12.
Costantini, M., Ferretti, A., Minati, F., Falco, S., Trillo, F., Colombo, D., Novali, F., Malvarosa, F., Mammone, F., Vecchioli, F., Rucci, A., Fumagalli, A., Allievi, J., Ciminelli, M., Costabile, S., 2017. Analysis of surface deformations over the whole Italian territory by interferometric processing of ERS, Envisat and COSMO-SkyMed radar data. Remote Sens. Environ. 202, 250–275. https://doi.org/10.1016/j.rse.2017.07.017G.
Crescenti, U., Dramis, F., Gentili, B., Pambianchi, G., 1987. Deformazioni gravitative profonde di versante e grandi frane nell'area a Sud di Monte Porrara (Appennino centrale, Abruzzo). Mem. Soc. Geol. Ital. 39, 477–486.
Crosta, G.B., Frattini, P., Agliardi, F., 2013. Deep seated gravitational slope deformations in the European Alps. Tectonophysics 605, 13–33. https://doi.org/10.1016/j.tecto.2013.04.028.
D'Agostino, N., Jackson, J.A., Dramis, F., Funiciello, R., 2001. Interactions between mantle upwelling, drainage evolution and active normal faulting: an example from the central Apennines (Italy). Geophys. J. Int. 147, 475–497. https://doi.org/10.1046/j.1365-246X.2001.00539.x.
Del Rio, L., Moro, M., Fondriest, M., Saroli, M., Goris, Falcucci, E., Cavallo, A., Doumaz, F., Di Toro, G., 2021. Active faulting and deep-seated gravitational slope deformation in carbonate rocks (central Apennines, Italy): a new "close-up" view. Tectonics 40, e2021TC006698. https://doi.org/10.1029/2021TC006698.
Delchiaro, M., Mele, E., Della Seta, M., Martino, S., Mazzanti, P., Esposito, C., 2021. Quantitative investigation of a mass rock creep deforming slope through A-Din SAR and geomorphometry. In: Vilímek, V., Wang, F., Strom, A., Sassa, K., Bobrowsky, P. T., Takara, K. (Eds.), Understanding and Reducing Landslide Disaster Risk. WLF 2020, ICL Contribution to Landslide Disaster Risk Reduction. Springer, Cham. https://doi.org/10.1007/978-3-030-60319-9_18.
Della Seta, M., Esposito, C., Marmoni, G.M., Martino, S., Scarascia Mugnozza, G., Troiani, F., 2017. Morpho-structural evolution of the valley-slope systems and related implications on slope-scale gravitational processes: new results from the Mt. Genzana case history (Central Apennines). Geomorphology 289, 60–77. https://doi.org/10.1016/j.geomorph.2016.07.003.
Di Luzio, E., Saroli, M., Esposito, C., Bianchi Fasani, G., Cavinato, G.P., Scarascia Mugnozza, G., 2004a. Influence of structural framework on mountain slope deformation in the Maiella anticline (Central Apennines, Italy). Geomorphology 60, 417–432. https://doi.org/10.1016/j.geomorph.2003.10.004.
Di Luzio, E., Bianchi Fasani, G., Saroli, M., Esposito, C., Cavinato, G.P., Scarascia Mugnozza, G., 2004b. Massive rock slope failure in the central Apennines (Italy): the case of the Campo di Giove rock avalanche. Bull. Eng. Geol. Environ. 63, 1–12. https://doi.org/10.1007/s10064-003-0212-7.
Di Luzio, E., Mele, G., Tiberti, M.M., Cavinato, G.P., Parotto, M., 2009. Moho deepening and shallow upper crustal delamination beneath the central Apennines. Earth Planet. Sci. Lett. 280, 1–12. https://doi.org/10.1016/j.epsl.2008.09.018.
Di Martire, D., Novellino, A., Ramondini, M., Calcaterra, D., 2016. A-Differential Synthetic Aperture Radar Interferometry analysis of a Deep-Seated Gravitational Slope Deformation occurring at Bisaccia (Italy). Sci. Total Environ. 550, 556–573. https://doi.org/10.1016/j.scitotenv.2016.01.102.
Di Martire, D., Paci, M., Confuorto, P., Costabile, S., Guastaferro, F., Verta, A., Calcaterra, D., 2017. A nation-wide system for landslide mapping and risk management in Italy: the second Not-ordinary Plan of Environmental Remote Sensing. Int. J. Appl. Earth Obs. Geoinf. 63, 143–157. https://doi.org/10.1016/j.jag.2017.07.018.
Di Naccio, D., Famiani, D., Liberi, F., Boncio, P., 2020. Site effects and widespread susceptibility to permanent coseismic deformation in the Avezzano town (Fucino basin, Central Italy): constraints from detailed geological study. Eng. Geol. 270, 105583 https://doi.org/10.1016/j.enggeo.2020.10558.3.
Discenza, M.E., Esposito, C., 2021. State-of-art and remarks on some open questions about DSGSDs: hints from a review of the scientific literature on related topics. Ital. J. Eng. Geol. Environ. 21 (1), 31–59. https://doi.org/10.4408/IJEGE.2021-01.O-03.
Discenza, M.E., Esposito, C., Martino, S., Petitta, M., Prestininzi, A., Scarascia Mugnozza, G., 2011. The gravitational slope deformation of Mt. Rocchetta ridge (central Apennines, Italy): geological-evolutionary model and numerical analysis. Bull. Eng. Geol. Environ. 70 (4), 559–575. https://doi.org/10.1007/s10064-010-0342-7.
Discenza, M.E., Martino, S., Bretschneider, A., Scarascia Mugnozza, G., 2020. Influence of joints on creep processes involving rock masses: results from physical-analogue laboratory tests. Int. J. Rock Mech. Min. Sci. 128, 104261 https://doi.org/10.1016/j.ijrmms.2020.104261.
Discenza, M.E., Esposito, C., Komatsu, G., Miccadei, E., 2021. Large-scale and deep-seated gravitational slope deformations on Mars: a review. Geosciences 11 (4), 174. https://doi.org/10.3390/geosciences11040174.
Dramis, F., Sorriso-Valvo, M., 1994. Deep-seated gravitational slope deformations, related landslides and tectonics. Eng. Geol. 38, 231–243.
Dramis, F., Gentili, B., Pambianchi, G., 1987. Deformazioni gravitative profonde nell'area di Monte Gorzano (Monti della Laga, Appennino Centrale). Boll. Soc. Geol. It. 106, 265–271.
Esposito, C., Martino, S., Scarascia Mugnozza, G., 2007. Mountain slope deformations along thrust fronts in jointed limestone: an equivalent continuum modelling approach. Geomorphology 90, 55–72. https://doi.org/10.1016/j.geomorph.2007.01.017.
Esposito, C., Bianchi Fasani, G., Martino, S., Scarascia Mugnozza, G., 2013. Quaternary gravitational morpho-genesis of central Apennines (Italy): insights from the Mt Genzana case history. Tectonophysics 605, 96–103. https://doi.org/10.1016/j.tecto.2013.06.023.
Esposito, C., Di Luzio, E., Scarascia Mugnozza, G., Bianchi Fasani, G., 2014. Mutual interactions between slope-scale gravitational processes and morpho-structural evolution of central Apennines (Italy): review of some selected case histories. Rendiconti Lincei 25, 151–165. https://doi.org/10.1007/s12210-014-0348-3.
Esposito, C., Di Luzio, E., Baleani, M., Troiani, F., Della Seta, M., Bozzano, F., Mazzanti, P., 2021. Fold architecture predisposing deep-seated gravitational slope deformations within a flysch sequence in the Northern Apennines (Italy). Geomorphology 380, 107629. https://doi.org/10.1016/j.geomorph.2021.107629.
Faccenna, C., Becker, T.W., Miller, M.S., Serpelloni, E., Willett, S.D., 2014. Isostasy, dynamic topography, and the elevation of the Apenninees of Italy. Earth Planet. Sci. Lett. 407, 163–174. https://doi.org/10.1016/j.epsl.2014.09.027.
Franceschetti, G., Migliaccio, M., Riccio, D., Schirinzi, G., 1992. SARAS: a synthetic aperture radar (SAR) raw signal simulator. IEEE Trans. Geosci. Remote Sensing 30, 110–123. https://doi.org/10.1109/36.124221.
Frattini, P., Crosta, G.B., Allievi, J., 2013. Damage to buildings in large slope rock instabilities monitored with the PSInSARTM technique. Remote Sens. 5, 4753–4773. https://doi.org/10.3390/rs5104753.
Frattini, P., Crosta, G.B., Rossini, M., Allievi, J., 2018. Activity and kinematic behaviour of deep-seated landslides from PS-InSAR displacement rate measurements. Landslides 15 (6), 1053–1070. https://doi.org/10.1007/s10346-017-0940-6.
Galadini, G., 2006. Quaternary tectonics and large-scale gravitational deformations with evidence of rock-slide displacements in the Central Apennines (central Italy). Geomorphology 82, 201–228. https://doi.org/10.1016/j.geomorph.2006.05.003.
Galadini, F., Galli, P., 1999. The Holocene paleoearthquakes on the 1915 Avezzano earthquake faults (central Italy): implications for active tectonics in the central Apennines. Tectonophysics 308, 143–170. https://doi.org/10.1016/S0040-1951(99)00091-8.
Galadini, F., Messina, P., 1994. Plio-Quaternary tectonics of the Fucino basin and surrounding areas (central Italy). Giornale Geol. Ser. 3 56 (2), 73–99.
Galadini, F., Messina, P., Giaccio, B., Sposato, A., 2003. Early uplift history of the Abruzzi Apennines (central Italy): available geomorphological constraints. Quat. Int. 101–102, 125–135. https://doi.org/10.1016/S1040-6182(02)00095-2.
Geoportale Nazionale, 2017. Ministero dell'Ambiente e della Tutela del Territorio e del Mare. http://www.pcn.minambiente.it/mattm.
Giraudi, C., 1988. Evoluzione geologica della Piana del Fucino (Abruzzo) negli ultimi 30.000 anni. Il Quaternario. Ital. J. Quaternary Sci. 1 (2), 131–159.
Gori, S., Falcucci, E., Dramis, F., Galadini, F., Galli, P., Giaccio, B., Messina, P., Pizzi, A., Sposato, A., Cosentino, D., 2014. Deep-seated gravitational slope deformation, large-scale rock failure, and active normal faulting along Mt. Morrone (Sulmona basin, central Italy): geomorphological and paleoseismological analyses. Geomorphology 208, 88–101. https://doi.org/10.1016/j.geomorph.2013.11.017.
Guallini, L., Brozzetti, F., Marinangeli, L., 2012. Large-scale deformational systems in the South Polar Layered Deposits (Promethei Lingula, Mars): "soft-sediment" and deep-seated gravitational slope deformations mechanisms. Icarus 220, 821–843. https://doi.org/10.1016/j.icarus.2012.06.023.
Hoek, E., Brown, E.T., 1997. Practical estimates of rock mass strength. Int. J. Rock Mech. Min. Sci. 34 (8), 1165–1186.
Hutchinson, J.N., 1988. General report: Morphological and geotechnical parameters of landslides in relation to geology and hydrogeology. In: Bonnard, C. (Ed.), Proceedings of the 5th International Symposium on Landslides, Lausanne 1988. Balkema, Rotterdam.
Iglesias, R., Mallorqui, J.J., Monells, D., López-Martínez, C., Fabregas, X., Aguasca, A., Gill, J.A., Corominas, J., 2015. PSI deformation map retrieval by means of temporal Sublook coherence on reduced sets of SAR images. Remote Sens. 7 (1), 530–563. https://doi.org/10.3390/rs70100530.
Jaboyedoff, M., Penna, I., Pedrazzini, A., Baron, I., Crosta, G.B., 2013. An introducing review on gravitational-deformation induced structures, fabrics and modeling. Tectonophysics 605, 1–12. https://doi.org/10.1016/j.tecto.2013.06.027.
Lenti, L., Martino, S., Paciello, A., Prestininzi, A., Rivellino, S., 2012. Microseismicity within a karsified rock mass due to cracks and collapses triggered by earthquakes and gravitational deformations. Nat. Hazards 64, 359–379. https://doi.org/10.1007/s11069-012-0245-y.

Madritsch, H., Millen, B.M.J., 2007. Hydrogeologic evidence for a continuous basal shear zone within a deep-seated gravitational slope deformation (Eastern Alps, Tyrol, Austria). Landslides 4, 149–162. https://doi.org/10.1007/s10346-006-0072-x.

Maffei, A., Martino, S., Prestininzi, A., 2005. From the geological to the numerical model in the analysis of gravity-induced slope deformations: an example from the Central Apennines (Italy). Eng. Geol. 78, 215–236. https://doi.org/10.1016/j.enggeo.2004.12.009.

Mahr, T., 1977. Deep-reaching gravitational deformations of high mountain slopes. Bull. Int. Ass. Engin. Geol. 16, 121–127.

Martino, S., Prestininzi, A., Scarascia Mugnozza, G., 2004. Geological-evolutionary model of a gravity-induced slope deformation in the carbonate central Apennines (Italy). Q. J. Eng. Geol. Hydrogeol. 37, 31–47. https://doi.org/10.1144/1470-9236/03-030.

Martino, S., Cercato, M., Della Seta, M., Esposito, C., Hailemikael, S., Iannucci, R., Martini, G., Paciello, A., Scarascia Mugnozza, G., Seneca, D., Troiani, F., 2020. Relevance of rock slope deformations in local seismic response and microzonation: insights from the Accumoli case-study (central Apennines, Italy). Eng. Geol. 266, 105427 https://doi.org/10.1016/j.enggeo.2019.105427.

Mège, D., Bourgeois, O., 2011. Equatorial glaciations on Mars revealed by gravitational collapse of Valles Marineris wallslopes. Earth Planet. Sci. Lett. 310, 182–191. https://doi.org/10.1016/j.epsl.2011.08.030.

Mora, O., Mallorqui, J.J., Broquetas, A., 2003. Linear and nonlinear terrain deformation maps from a reduced set of interferometric sar images. IEEE Trans. Geosci. Remote Sens. 41 (10), 2243–2253. https://doi.org/10.1109/TGRS.2003.814657.

Moreira, J., Schwabisch, M., Fornaro, G., Lanari, R., Bamler, R., Just, D., Steinbrecher, U., Breit, H., Eineder, M., Franceschetti, G., Geudtner, D., Rinkel, H., 1995. X-SAR interferometry: first results. IEEE Trans. Geosci. Remote Sens. 33 (4), 950–956.

Moro, M., Saroli, M., Salvi, S., Stramondo, S., Doumaz, F., 2007. The relationship between seismic deformation and deep-seated gravitational movements during the 1997 Umbria-Marche (Central Italy) earthquakes. Geomorphology 89, 297–307. https://doi.org/10.1016/j.geomorph.2006.12.013.

Moro, M., Saroli, M., Tolomei, C., Salvi, S., 2009. Insights on the kinematics of deep-seated gravitational slope deformations along the 1915 Avezzano earthquake fault (central Italy), from time-series DInSAR. Geomorphology 112, 261–276. https://doi.org/10.1016/j.geomorph.2009.06.011.

Moro, M., Saroli, M., Gori, S., Falcucci, E., Galadini, F., Messina, P., 2012. The interaction between active normal faulting and large-scale gravitational mass movements revealed by paleoseismological techniques: a case study from central Italy. Geomorphology 151-152, 164–174. https://doi.org/10.1016/j.geomorph.2012.01.026.

Nemčok, A., 1972. Gravitational slope deformation in high mountains. In: Proceedings of the 24th International Geological Congress, Montreal, Sect 13, pp. 132–141.

Nijman, W., 1971. Tectonics of the Velino - Sirente area, Abruzzi, Central Italy. Koninkl. Nederl. Akad. van Wetenshappen Proc. B 74 (2), 156–184.

Notti, D., Meisina, C., Colombo, A., Lanteri, L., Zucca, F., 2013. Studying and monitoring large landslides with persistent scatterer data. Ital. J. Eng. Geol. Environ. 6, 349–360. https://doi.org/10.4408/IJEGE.2013-06.B-33.

Pánek, T., Klimeš, J., 2016. Temporal behaviour of deep-seated gravitational slope deformations: a review. Earth-Sci. Rev. 156, 14–38. https://doi.org/10.1016/j.earscirev.2016.02.007.

Patacca, E., Scandone, P., Di Luzio, E., Cavinato, G.P., Parotto, M., 2008. Structural architecture of the central Apennines. Interpretation of the CROP 11 seismic profile from the Adriatic coast to the orographic divide. Tectonics 27, TC3006. https://doi.org/10.1029/2005TC001917.

Plank, S., Singer, J., Minet, C., Thuro, K., 2012. Pre-survey suitability evaluation of the differential synthetic aperture radar interferometry method for landslide monitoring. Int. J. Remote Sens. 33 (20), 6623–6637. https://doi.org/10.1080/01431161.2012.693646.

Praturlon, A., 1968. Note illustrative alla Carta Geologica d'Italia, foglio 152 - Sora (scala 1:100.000). Poligrafica e Carta valori Ercolano, Napoli (76 pp.).

Radbruch-Hall, D., 1978. Gravitational creep of rock masses slopes. In: Voight, B. (Ed.), Rockslides and Avalanches, Natural Phenomena 1, Development in Geotechnical Engineering 14 (Part A), pp. 607–657.

Sacco, P., Battagliere, M.L., Daraio, M.G., Coletta, A., 2015. The COSMO-SkyMed constellation monitoring of the Italian territory: the Map Italy project. In: Proc. of 66th International Astronautical Congress (IAC 2015), pp. 12–16.

Scarascia Mugnozza, G., Bianchi Fasani, G., Esposito, C., Martino, S., Saroli, M., Di Luzio, E., Evans, S.G., 2006. Rock avalanche and mountain slope deformation in a convex dip-slope: the case of the Maiella massif, Central Italy. In: Evans, S.G., Scarascia Mugnozza, G., Strom, A., Hermanns, R. (Eds.), Massive Rock Slope Failure. Kluwer Academic Publishers, Dordrecht. https://doi.org/10.1007/978-1-4020-4037-5_19. ISBN, 978-1-4020-4035-1.

Solari, L., Del Soldato, M., Raspini, F., Barra, A., Bianchini, S., Confuorto, P., Casagli, N., Crosetto, M., 2020. Review of satellite interferometry for landslide detection in Italy. Remote Sens. 12 (8), 1351. https://doi.org/10.3390/rs12081351.

Sorriso-Valvo, M., 1995. Considerazioni sul limite tra deformazione gravitativa di versante e frana. Mem. Soc. Geol. It. 50, 179–185.

Strauhal, T., Zangerl, C., Fellin, W., Holzmann, M., Engl, D.A., Brandner, R., Tropper, P., Tessadri, R., 2017. Structure, mineralogy and geomechanical properties of Shear zones of Deep-Seated Rockslides in metamorphic rocks (Tyrol, Austria). Rock Mech. Rock. Eng. 50 (2), 419–438. https://doi.org/10.1007/s00603-016-1113-y.

Zangerl, C., Eberhardt, E., Perzlmaier, S., 2010. Kinematic behaviour and velocity characteristics of a complex deep-seated crystalline rockslide in relation to its interaction with a dam reservoir. Eng. Geol. 112, 53–67. https://doi.org/10.1016/j.enggeo.2010.01.001.

Zischinsky, U., 1966. On the deformation of high slopes. In: Proceeding of the 1st Conf. of the International Society of Rock Mechanics, Lisbon, 2, pp. 179–185.